

Fairness under Graph Uncertainty: Achieving Interventional Fairness with Partially Known Causal Graphs over Clusters of Variables

Yoichi Chikahara¹

¹NTT Communication Science Laboratories, Kyoto, Japan

Abstract

Algorithmic decisions about individuals require predictions that are not only accurate but also fair with respect to sensitive attributes such as gender and race. Causal notions of fairness align with legal requirements, yet many methods assume access to detailed knowledge of the underlying causal graph, which is a demanding assumption in practice. We propose a learning framework that achieves interventional fairness by leveraging a causal graph over *clusters of variables*, which is substantially easier to estimate than a variable-level graph. With possible *adjustment cluster sets* identified from such a cluster causal graph, our framework trains a prediction model by reducing the worst-case discrepancy between interventional distributions across these sets. To this end, we develop a computationally efficient barycenter kernel maximum mean discrepancy (MMD) that scales favorably with the number of sensitive attribute values. Extensive experiments show that our framework strikes a better balance between fairness and accuracy than existing approaches, highlighting its effectiveness under limited causal graph knowledge.

Nevertheless, achieving causality-based fairness remains challenging. Most existing methods assume access to the ground-truth causal graph over an individual’s features [Kusner et al., 2017, Chiappa and Gillam, 2019, Salimi et al., 2019, Chikahara et al., 2021]. In the absence of perfect domain knowledge, this assumption forces us to solve the notoriously difficult problem of learning the entire causal graph structure from observational data—even though our ultimate objective is simply to ensure fairness. Moreover, learning the full graph relies on restrictive functional assumptions about the data-generating process [Glymour et al., 2019], and their violations can undermine fairness guarantees.

To relax these demanding assumptions, recent methods leverage a *completed partially directed acyclic graph* (CPDAG), which is identifiable from conditional independence relations [Li et al., 2024, Zuo et al., 2024]. These methods aim to achieve a causality-based notion called *interventional fairness* [Salimi et al., 2019] by inferring interventional distributions of the predictions under interventions on sensitive features based on a CPDAG. However, estimating a CPDAG remains challenging in high-dimensional settings: it typically requires a large number of conditional independence tests, so estimation errors can accumulate and ultimately undermine the reliability of fairness guarantees.

The goal of this paper is to ensure interventional fairness in more realistic scenarios where we only have access to a *cluster CPDAG* [Anand et al., 2025], i.e., a CPDAG defined over clusters of variables formed according to a user-specified partition. Since such clustering reduces the graph size, cluster CPDAG inference needs substantially fewer conditional independence tests than variable-level CPDAG inference [Tikka et al., 2023, Anand et al., 2025]. This crucial advantage motivates our research question: *Can we achieve interventional fairness using a cluster CPDAG, despite the causal structure inside each cluster being unknown?*

We answer yes with the following **key contributions**:

- We develop a graphical algorithm to enumerate *adjustment cluster sets*, at least one of which enables the

1 INTRODUCTION

Machine learning is increasingly used to automate high-stakes decisions about individuals, such as hiring and lending [Houser, 2019, Fuster et al., 2022]. However, the substantial societal impact of such algorithmic decisions raises concerns about *discrimination* with respect to sensitive attributes such as gender and race. Because discrimination is often legally assessed based on the causal relationship between a challenged decision and sensitive attributes, many causality-based fairness notions have been proposed [Kusner et al., 2017, Salimi et al., 2019, Wu et al., 2019].

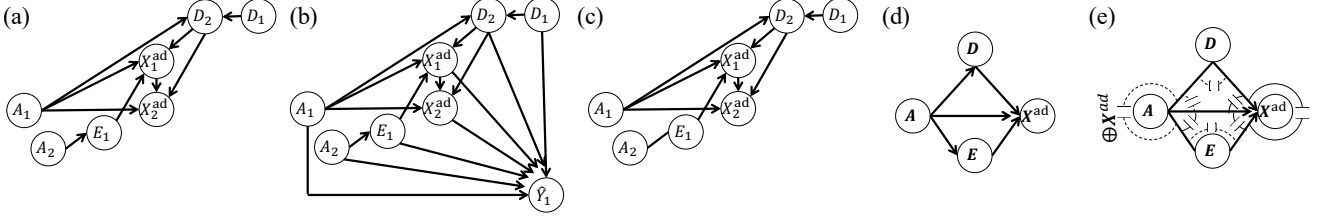


Figure 1: Causal graphs representing a scenario of hiring decisions: (a) DAG over X , (b) DAG over X and \hat{Y} , (c) CPDAG over X , (d) cluster DAG over X , and (e) cluster CPDAG over X with independence arcs and connection/separation marks.

identification of interventional distributions for the true cluster DAG compatible with the cluster CPDAG.

- We propose a learning framework that achieves interventional fairness by penalizing the *worst-case* unfairness across these adjustment cluster sets. To efficiently measure the overall discrepancy across pairs of interventional distributions, we introduce a computationally efficient barycenter kernel maximum mean discrepancy (MMD) that scales favorably with both the number of sensitive attribute values and the sample size.
- Through extensive experiments on synthetic and real-world datasets, we demonstrate that the proposed method attains a better trade-off between fairness and predictive accuracy than existing approaches.

2 PRELIMINARIES

2.1 PROBLEM SETUP

We consider (possibly multi-output) supervised learning. We train a model h_θ with parameters θ that outputs prediction \hat{Y} of decision outcome(s) Y from each individual's features X , including discrete-valued sensitive features A .

We seek parameters θ that achieve a good balance between prediction accuracy and fairness with respect to sensitive features A . Given n training instances $\{(\mathbf{x}_i, \mathbf{y}_i)_{i=1}^n\}$, our learning problem is formulated as

$$\min_{\theta} \frac{1}{n} \sum_{i=1}^n \ell(\mathbf{y}_i, h_\theta(\mathbf{x}_i)) + \lambda g_\theta(\mathbf{x}_1, \dots, \mathbf{x}_n), \quad (1)$$

where ℓ is a loss function that measures the prediction error, g_θ is a penalty function that quantifies the unfairness of predictive model h_θ , and $\lambda \geq 0$ is a hyperparameter.

We formulate penalty function g_θ based on the notion of interventional fairness [Salimi et al., 2019], which is defined using structural causal models (SCMs) [Pearl, 2009].

2.2 FAIRNESS VIA LENS OF CAUSALITY

Consider a scenario of making hiring decisions for physically demanding jobs [Chikahara et al., 2023]. We predict $\hat{Y} = [\hat{Y}_1]$ from each applicant's features $X =$

$\{A, X^{\text{ad}}, D, E\}$: gender and nationality $A = [A_1, A_2]$ (sensitive features), physical test scores $X^{\text{ad}} = [X_1^{\text{ad}}, X_2^{\text{ad}}]$, medical test results $D = [D_1, D_2]$, and educational background $E = [E_1]$. Since the job requires physical strength, we treat the physical test scores X^{ad} as *admissible* features, whose use in decision-making is **not** regarded as indirect discrimination with respect to the sensitive features A .

When causal relationships among features X are expressed by the *causal graph* in Figure 1(a), we can depict the data-generating process of X and \hat{Y} as in Figure 1(b) by adding directed edges from each feature in X to prediction \hat{Y} .

An SCM formalizes such data-generating process. For example, physical test score X_1^{ad} is determined by the values of its *parents* in the causal graph in Figure 1(b):

$$X_1^{\text{ad}} = f_{X_1^{\text{ad}}}(A_1, D_2, E_1, U_{X_1^{\text{ad}}}), \quad (2)$$

where $U_{X_1^{\text{ad}}}$ is an exogenous noise, and $f_{X_1^{\text{ad}}}$ is a deterministic function. Whereas the true forms of such deterministic functions as $f_{X_1^{\text{ad}}}$ are unknown for observed features X , the prediction $\hat{Y} = [\hat{Y}_1]$ is given by the known function, as it is produced by a prediction model h_θ :

$$\hat{Y} = h_\theta(X, U_{\hat{Y}}), \quad (3)$$

where $U_{\hat{Y}}$ is an exogenous noise term corresponding to the randomness of h_θ when it is a probabilistic model.

Interventional fairness is defined via an operation on an SCM called an *intervention*. For instance, an intervention $do(X_1^{\text{ad}} = x_1^{\text{ad}})$ modifies the data-generating process of X_1^{ad} in (2) by forcing X_1^{ad} to take the fixed value x_1^{ad} . Using such hypothetical modifications to the data-generating process, interventional fairness is defined as the equality of the *interventional distributions* of \hat{Y} under interventions on the sensitive features A and the admissible features X^{ad} :

Definition 2.1 (Salimi et al. [2019]). Prediction \hat{Y} is *interventionally fair* with respect to sensitive features A , if

$$\begin{aligned} & \mathbb{P}(\hat{Y} = \hat{y} \mid do(A = \mathbf{a}), do(X^{\text{ad}} = \mathbf{x}^{\text{ad}})) \\ &= \mathbb{P}(\hat{Y} = \hat{y} \mid do(A = \mathbf{a}'), do(X^{\text{ad}} = \mathbf{x}^{\text{ad}})), \end{aligned} \quad (4)$$

holds for all possible prediction values \hat{y} , for any discrete values \mathbf{a}, \mathbf{a}' of sensitive features A and for any discrete values \mathbf{x}^{ad} of admissible features X^{ad} .

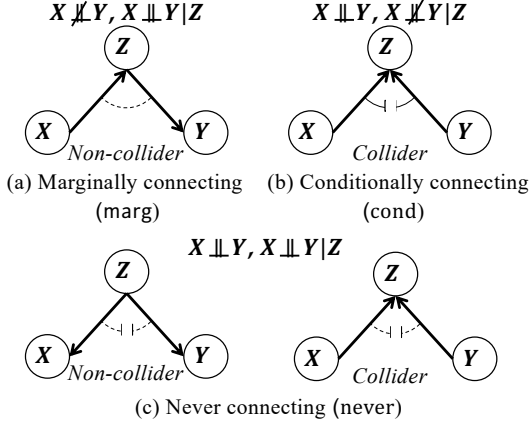


Figure 2: Independence arcs for cluster triplet $\langle X, Z, Y \rangle$

Remark 2.2 (Connection to other causality-based notions). Unlike *counterfactual fairness* [Kusner et al., 2017, Wu et al., 2019], interventional fairness is (i) a *group-level* notion—in contrast to *individual-level* one, which is formalized via conditional distributions conditioned on all features X of an individual—and (ii) defined using interventional distributions, not counterfactual distributions [Pearl, 2009].

An advantage of interventional fairness is that the interventional distributions in Eq. (4) can be identified using partial causal graph knowledge, formalized as a CPDAG [Maathuis et al., 2009, Fang and He, 2020, Guo and Perković, 2022].

A CPDAG represents a *Markov equivalence class* (MEC), a class of causal DAGs with the same conditional independence relations among variables. It contains directed edges that are common to all DAGs in the class, and undirected edges whose orientations vary across the DAGs. For example, the MEC containing the causal DAG in Figure 1 (a) is given by the CPDAG in Figure 1 (c), where the directed edges in collider structures (e.g., $A_1 \rightarrow X_1^{\text{ad}} \leftarrow E_1$ with A_1 and E_1 being non-adjacent (i.e., *unshielded*)) remain directed, since their conditional independence relations differ from those in non-collider structures.

Although CPDAG inference only requires conditional independence tests, it can be challenging in high-dimensional setups due to the large number of tests required. This challenge motivates *cluster causal graphs*, as their estimation needs exponentially fewer tests (with respect to the maximum node degree) and can further gain statistical power by leveraging modern multivariate testing [Anand et al., 2025].

2.3 CLUSTER CAUSAL GRAPHS

Cluster DAGs A cluster graph G is constructed by grouping nodes \mathcal{V} in a variable-level DAG $G_{\mathcal{V}}$ [Anand et al., 2023]. Given a partition of d clusters $\mathcal{C} = \{C_1, \dots, C_d\}$ of nodes \mathcal{V} , a cluster graph G over \mathcal{C} has a directed edge $C_i \rightarrow C_j$ between clusters $C_i, C_j \in \mathcal{C}$, if some $V_i \in C_i$ and $V_j \in C_j$

have edge $V_i \rightarrow V_j$ in $G_{\mathcal{V}}$. For instance, the causal graph in Figure 1 (a) is converted to the cluster DAG in Figure 1 (d). Following Anand et al. [2025], we assume that the resulting cluster graph is a DAG; this assumption is feasible for many applications by leveraging domain knowledge to design an appropriate partition, called an *admissible partition*.

Even under acyclicity, a cluster graph can entail different conditional independence relations among the clusters, depending on the unspecified variable-level structures within each cluster. For example, as illustrated in Figure 2 (b) and (c; right), collider structure $X \rightarrow Z \leftarrow Y$ can entail different relations $X \not\perp Y | Z$ and $X \perp Y | Z$, depending on whether variable-level collider structure $X_i \rightarrow Z_k \leftarrow Y_j$ exists in $G_{\mathcal{V}}$ for some $X_i \in X, Y_j \in Y$, and $Z_k \in Z$.

To explicitly represent such differences, Anand et al. [2025] propose *independence arcs*, as well as *connection* and *separation* marks. An independence arc $\mathcal{A}_{\langle X, Z, Y \rangle}$ over an (unshielded) cluster triplet $\langle X, Z, Y \rangle$ takes three possible states: *marginally connecting* (marg), *conditionally connecting* (cond), and *never connecting* (never), each implying the conditional independence relations described in Figure 2. A connection mark $\oplus C$ and a separation mark $\ominus C$ for some cluster set $C \subseteq \mathcal{C}$ are put on independence arc $\mathcal{A}_{\langle X, Z, Y \rangle}$, if conditioning C renders X and Y dependent and independent, respectively, which are otherwise not implied by the state of arc $\mathcal{A}_{\langle X, Z, Y \rangle}$. We present the definitions in Section A.2.

Cluster CPDAGs A cluster CPDAG expresses a *cluster MEC*, a class of cluster DAGs with identical conditional independence relations among clusters. As in Figure 1 (e), it contains directed edges, independence arcs, and connection/separation marks shared in all cluster DAGs in the class, and undirected edges whose orientations differ in the class.

Anand et al. [2025] propose the inference method for a cluster CPDAG, called the *causal learning over clusters* (CLOC). Compared to other algorithms for learning cluster graphs [Segal et al., 2005, Tikka et al., 2023, Wahl et al., 2024], it does not require restrictive assumptions about the underlying graph structure (e.g., the connectivity of nodes within each cluster). For this reason, we build upon CLOC to achieve interventional fairness using a cluster CPDAG.

3 PROPOSED METHOD

We propose a framework for achieving interventional fairness (Definition 2.1) using an inferred cluster CPDAG.

3.1 CHALLENGES IN CLUSTER CPDAGS

To ensure interventional fairness, we design penalty function g_{θ} in (1) that reduces the discrepancy between interventional distributions in (4). However, when only a cluster CPDAG is available, inferring these distributions is challenging.

If we have access to the variable-level causal DAG, we can infer interventional distributions by identifying adjustment variables \mathbf{Z} from the graph structure and marginalizing over \mathbf{Z} and the remaining variables $\mathbf{X}^{\text{re}} = \mathbf{X} \setminus \{\mathbf{A}, \mathbf{X}^{\text{ad}}, \mathbf{Z}\}$:

$$\begin{aligned} & \mathbb{P}(\hat{\mathbf{Y}} = \hat{\mathbf{y}} \mid do(\mathbf{A} = \mathbf{a}), do(\mathbf{X}^{\text{ad}} = \mathbf{x}^{\text{ad}})) \\ &= \mathbb{E}_{\mathbf{Z}, \mathbf{X}^{\text{re}} \mid \mathbf{a}, \mathbf{x}^{\text{ad}}} \left[\mathbb{P}(\hat{\mathbf{Y}} = \hat{\mathbf{y}} \mid \mathbf{A} = \mathbf{a}, \mathbf{X}^{\text{ad}} = \mathbf{x}^{\text{ad}}, \mathbf{Z}, \mathbf{X}^{\text{re}}) \right]. \end{aligned} \quad (5)$$

This expectation can be estimated from the data distribution.

However, since a cluster CPDAG represents multiple DAGs (in the cluster MEC), we cannot identify such a single adjustment set \mathbf{Z} . A possible solution is to enumerate adjustment sets $\mathbf{Z}^1, \dots, \mathbf{Z}^M$, such that, for any cluster DAG in the cluster MEC, at least one set enables the adjustment in Eq. (5).

In case of variable-level CPDAGs, we can efficiently enumerate such adjustment sets [Li et al., 2024], thanks to the desirable graphical properties (e.g., chordality of *chain components*, each connected with undirected edges [Guo and Perković, 2022]). However, cluster CPDAGs do not enjoy these ideal properties, and their graph structures alone are insufficient to determine conditional independence relations among clusters, as described in Section 2.3.

For this reason, we develop a novel adjustment set enumeration algorithm that explicitly accounts for independence arcs and separation/connection marks in a cluster CPDAG.

3.2 ADJUSTMENT SET ENUMERATION

3.2.1 Assumptions and Enumeration Strategy

Inferring a cluster CPDAG over features \mathbf{X} with the CLOC algorithm [Anand et al., 2025] requires three assumptions:

Assumption 3.1. The underlying variable-level causal graph over features \mathbf{X} is a DAG and contains no unobserved confounders between any pair of features in \mathbf{X} .

Assumption 3.2. A partition of clusters $\mathcal{C} = \{\mathcal{C}_1, \dots, \mathcal{C}_d\}$ is admissible: No directed cycle arises due to the partition.

Assumption 3.3. Distribution $\mathbb{P}(\mathcal{C})$ is faithful to the underlying cluster DAG over \mathcal{C} (See Section A.3 for details).

Violating these assumptions implies no guarantee to recover the true cluster CPDAG; however, we empirically observe that the resulting CPDAG is useful for enforcing fairness (Section E.3). Assuming acyclicity and no unobserved confounders, which is standard in the literature on interventional fairness [Li et al., 2024, Zuo et al., 2024], is sufficient to apply the standard *back-door adjustment* [Pearl, 2009].

For this reason, we seek adjustment sets $\mathbf{Z}^1, \dots, \mathbf{Z}^M$ such that, for the true cluster DAG, at least one of these sets *d-separates* all *back-door paths* from sensitive features \mathbf{A} to prediction $\hat{\mathbf{Y}}$ (i.e., the paths with $\mathbf{A} \leftarrow \dots$ connecting to $\hat{\mathbf{Y}}$). For this goal, we use the cluster-level d-separation:

Definition 3.4 (Anand et al. [2025]). A path $p = \langle \mathcal{C}_1, \mathcal{C}_2, \mathcal{C}_3, \dots, \mathcal{C}_d \rangle$ in a cluster DAG is d-separated by a set of clusters $\mathbf{Z} \subset \mathcal{C}$ if and only if the sequence of independence arcs along the path, $\mathcal{A}_{\langle \mathcal{C}_1, \mathcal{C}_2, \mathcal{C}_3 \rangle}, \dots, \mathcal{A}_{\langle \mathcal{C}_{d-2}, \mathcal{C}_{d-1}, \mathcal{C}_d \rangle}$, contains independence arc $\mathcal{A}_{\langle \mathcal{C}_i, \mathcal{C}_k, \mathcal{C}_j \rangle}$ for i, k, j that

1. is marg with (a) \mathcal{C}_k in \mathbf{Z} or (b) separation mark $\circlearrowleft \mathcal{C}_x$ for some \mathcal{C}_x on path p , where $x \in \{1, \dots, d\}$.
2. is cond with (a) \mathcal{C}_k and its true descendant \mathcal{C}_{td} (with directed path $\mathcal{C}_k \rightarrow \dots \rightarrow \mathcal{C}_{\text{td}}$) not in \mathbf{Z} , and (b) has no connection mark $\oplus \mathcal{C}_x$ such that \mathcal{C}_x in \mathbf{Z} or (c) has separation mark $\circlearrowleft \mathcal{C}_x$ for some \mathcal{C}_x on path p .
3. is never and has no connection mark $\oplus \mathcal{C}_x$ for \mathcal{C}_x in \mathbf{Z} .

Definition 3.4 extends d-separation using independence arcs and marks. Unlike the original one, even when triplet $\langle \mathcal{C}_i, \mathcal{C}_k, \mathcal{C}_j \rangle$ forms a collider structure, if arc $\mathcal{A}_{\langle \mathcal{C}_i, \mathcal{C}_k, \mathcal{C}_j \rangle}$ takes never (Figure 2(c)), then the path remains d-separated regardless of whether \mathcal{C}_k (or its descendants) is in \mathbf{Z} .

For a cluster set to d-separate back-door paths from \mathbf{A} to $\hat{\mathbf{Y}}$, it suffices to d-separate back-door paths from \mathbf{A} to each feature in \mathbf{X} for cluster DAGs over features \mathbf{X} , as their corresponding cluster CPDAG can be augmented with prediction $\hat{\mathbf{Y}}$, as shown in Figure 1(b). For simplicity, we consider back-door paths $\mathbf{A} \leftarrow \dots$; the same procedure applies to $\mathbf{X}^{\text{ad}} \leftarrow \dots$. We obtain the adjustment sets in two steps:

1. **Parent Enumeration** (Section 3.2.2): From possible DAG structures, we enumerate the parents of \mathbf{A} , i.e., the clusters that appear first on back-door paths. If all parent sets contain no connection-marked cluster, they achieve adjustment; otherwise, we proceed to Step 2.
2. **Adjustment Set Completion** (Section 3.2.3): We iteratively augment each adjustment-set candidate with additional clusters needed to d-separate back-door paths.

3.2.2 Parent Set Enumeration

The parent sets of sensitive features \mathbf{A} fall into two categories. One is *definite parents* $\text{pa}(\mathbf{A})$, which are parents of \mathbf{A} in all cluster DAGs in the cluster MEC, i.e., clusters with directed edges into \mathbf{A} in the cluster CPDAG. The other is *possible parents*, which are parents of \mathbf{A} in some but not all cluster DAGs in the cluster MEC, i.e., clusters with undirected edges adjacent to \mathbf{A} in the cluster CPDAG.

Hence, to enumerate all parent candidate sets of \mathbf{A} , it suffices to take the union of definite and possible parent sets as

$$\mathbf{Z}^m := \text{pa}(\mathbf{A}) \cup S^m \text{ for } m = 1, \dots, M, \quad (6)$$

where S^1, \dots, S^M are possible parent sets, with M increasing with the number of undirected edges incident to \mathbf{A} .

To identify possible parent set S^m in (6), we give necessary and sufficient conditions for a subset of *siblings* of \mathbf{A} (i.e., clusters with an undirected edge incident to \mathbf{A}) to be S^m :

Algorithm 1 Adjustment Cluster Completion ($\mathbf{Z}^m, \mathbf{A}, \mathcal{G}$)

Require: \mathbf{Z}^m, \mathbf{A} , and cluster CPDAG \mathcal{G} over X

- 1: $\mathbf{Z} \leftarrow \mathbf{Z}^m$ in Eq. (6); Processed $\leftarrow \emptyset$
- 2: $\mathbf{Z}_\oplus \leftarrow \mathbf{Z} \cap \{\mathbf{C}_x \text{ in } \oplus \mathbf{C}_x \text{ in } \mathcal{A}_{\langle P, Q, R \rangle} \text{ for all triples in } \mathcal{G}\}$
- 3: Queue $\leftarrow \{(\mathbf{P}, \mathbf{Q}) : \mathbf{P} \in \mathbf{Z}_\oplus; \mathbf{Q} \text{ adjacent to } \mathbf{P}; \mathbf{Q} \neq \mathbf{A}\}$
- 4: **while** Queue $\neq \emptyset$ **do**
- 5: pop (\mathbf{P}, \mathbf{Q}) from Queue
- 6: **if** $(\mathbf{P}, \mathbf{Q}) \in$ Processed **then**
- 7: **continue**
- 8: Processed \leftarrow Processed $\cup \{(\mathbf{P}, \mathbf{Q})\}$
- 9: **for each** \mathbf{R} adjacent to \mathbf{Q} in \mathcal{G} and $\mathbf{R} \neq \mathbf{P}$ **do**
- 10: **if** $\mathcal{A}_{\langle P, Q, R \rangle} = \text{marg}$ **then**
- 11: $\mathbf{Z} \leftarrow \mathbf{Z} \cup \{\mathbf{Q}\}$
- 12: **else if** $\mathcal{A}_{\langle P, Q, R \rangle} = \text{never}$ **then**
- 13: $\mathbf{Z} \leftarrow \mathbf{Z} \cup \{\mathbf{Q}\}$
- 14: **if** Some $\mathbf{P}_x \in \mathbf{Z}$ in $\oplus \mathbf{C}_x$ in $\mathcal{A}_{\langle P, Q, R \rangle}$ **then**
- 15: push (\mathbf{Q}, \mathbf{R}) into Queue
- 16: **else if** $\mathcal{A}_{\langle P, Q, R \rangle} = \text{cond}$ **then**
- 17: $\mathbf{E} \leftarrow \text{POSSDESC}(\mathcal{G}, \mathbf{Q}); \mathbf{E} \leftarrow \mathbf{Z} \cap \mathbf{E}$
- 18: **if** $\mathbf{E} \neq \emptyset$ and \mathbf{Z} has no cluster in $\circ \mathbf{C}_x$ in $\mathcal{A}_{\langle P, Q, R \rangle}$ **then**
- 19: **return** (FAIL)
- 20: **return** (\mathbf{Z} , OK)

Theorem 3.5: A set of clusters $S \subseteq \text{sib}(\mathbf{A}, \mathcal{G}) := \{\mathbf{C} \in \mathcal{C} : \mathbf{C} - \mathbf{A} \text{ in } \mathcal{G}\}$ in a cluster CPDAG \mathcal{G} is a possible parent set of \mathbf{A} if and only if it satisfies the following two conditions:

1. **Collider-structure compatibility:** All distinct $\mathbf{U}, \mathbf{V} \in S$ satisfy either (i) \mathbf{U} and \mathbf{V} are adjacent, or (ii) \mathbf{U} and \mathbf{V} are not adjacent and $\mathcal{A}_{\langle \mathbf{U}, \mathbf{A}, \mathbf{V} \rangle} = \text{never}$.
2. **No back-path condition:** Let \mathcal{G}_\rightarrow be the directed subgraph of \mathcal{G} obtained by removing all undirected edges. For every $\mathbf{U} \in S$ and every $\mathbf{V} \in \text{sib}(\mathbf{A}, \mathcal{G}) \setminus S$, there is no directed path from \mathbf{V} to \mathbf{U} in \mathcal{G}_\rightarrow .

See Section C for the proof. Collider-structure compatibility is needed to exclude the cases where orienting two undirected edges as collider structure $\mathbf{U} \rightarrow \mathbf{A} \leftarrow \mathbf{V}$ contradicts independence arc $\mathcal{A}_{\langle \mathbf{U}, \mathbf{A}, \mathbf{V} \rangle}$. No back-path condition prevents the creation of directed cycles by orientation.

If the resulting parent sets $\mathbf{Z}^m = \text{pa}(\mathbf{A}) \cup S^m$ for $m = 1, \dots, M$ contain no connection-marked cluster for any cluster triplet in the cluster CPDAG, then they are sufficient to achieve back-door adjustment. Otherwise, we need to complete each set \mathbf{Z}^m by adding additional clusters.

3.2.3 Adjustment Cluster Completion

Algorithm 1 shows our queue-based propagation procedure for augmenting each set \mathbf{Z} with the clusters required for d-separation. Using a queue initialized with the parents of \mathbf{A} that appear in connection marks, it repeatedly inspects local

triple annotations and expands \mathbf{Z} whenever the annotations indicate that additional conditioning clusters are needed to achieve d-separation. The returned \mathbf{Z} is a valid adjustment set for some cluster DAGs in the cluster MEC.

A notable difference from Definition 3.4 is that whereas its Condition 2 involves *true* descendants, line 17 approximates them as *possible* descendants $\text{POSSDESC}(\mathcal{G}, \mathbf{Q})$, which we define as the set of clusters reachable from \mathbf{Q} by orienting undirected edges away from \mathbf{Q} . This approximation is **inevitable** because a cluster CPDAG contains undirected edges, making the true descendant set unidentifiable. To provide a safeguard against such unidentifiable cases, Algorithm 1 explicitly returns FAIL (line 19).

Graph Refinement for Unidentifiable Cases. In these cases, we refine the cluster CPDAG by splitting clusters that appear in connection marks into singleton nodes, and then obtain adjustment sets using the refined graph. This refinement incurs an additional cost for re-estimating the cluster CPDAG; however, it is often negligible in practice compared with variable-level CPDAG estimation because the number of nodes and the node degree are typically much smaller (see Section E.5 for a time-complexity comparison).

In our experiments, the number of refinement steps needed was 0 or 1. Although this number depends on the provided cluster CPDAG (e.g., the node degrees), it is at most the number of clusters d , where we obtain a variable-level CPDAG and hence can always identify valid adjustment sets. Refinement can also help reduce the number of undirected edges and adjustment sets M , as discussed in Section E.2.

3.3 PENALIZING WORST-CASE UNFAIRNESS

Using the adjustment cluster sets $\mathbf{Z}^1, \dots, \mathbf{Z}^M$, we now construct the unfairness penalty g_θ in (1).

Because it is uncertain which $\mathbf{Z}^1, \dots, \mathbf{Z}^M$ yields valid adjustment for the true cluster DAG, we consider the *worst-case* unfairness over these sets, defined as the maximum of the discrepancy between interventional distributions. For each \mathbf{Z}^m we aggregate kernel MMDs [Gretton et al., 2012] between the interventional distribution pairs in (4), and then take the maximum across $m = 1, \dots, M$:

$$\max_m \sum_{x^{\text{ad}}} \sum_{a, a'} \text{MMD}_m(\mathbb{P}_{\hat{Y}|do(a), do(x^{\text{ad}})}, \mathbb{P}_{\hat{Y}|do(a'), do(x^{\text{ad}})}),$$

where $\text{MMD}_m(\cdot, \cdot)$ denotes the kernel MMD between the corresponding interventional distributions identified via \mathbf{Z}^m .

Unfortunately, this maximization is computationally prohibitive, requiring $\mathcal{O}(M N_A^2 N_{x^{\text{ad}}} n^2)$ time, where N_A and $N_{x^{\text{ad}}}$ are the cardinalities of the sensitive and admissible feature values, and n is the sample size. To address this issue, below we introduce our estimation strategies and derive a computationally efficient penalty function g_θ .

3.3.1 Towards Efficient MMD Estimation

Our estimation strategies are twofold. First, we reduce the quadratic time complexity $\mathcal{O}(N_A^2)$ to $\mathcal{O}(N_A)$ by decomposing the summation over pairwise MMDs for sensitive feature values \mathbf{a} and \mathbf{a}' as the sum of *barycenter* MMDs:

$$\begin{aligned} & \sum_{\mathbf{a}, \mathbf{a}'} \text{MMD}_m(\mathbb{P}_{\hat{Y}|do(\mathbf{a}), do(\mathbf{x}^{ad})}, \mathbb{P}_{\hat{Y}|do(\mathbf{a}'), do(\mathbf{x}^{ad})}) \quad (7) \\ & = c \sum_{\mathbf{a}} \text{MMD}_m(\mathbb{P}_{\hat{Y}|do(\mathbf{a}), do(\mathbf{x}^{ad})}, \frac{1}{N_A} \sum_{\mathbf{a}'} \mathbb{P}_{\hat{Y}|do(\mathbf{a}'), do(\mathbf{x}^{ad})}), \end{aligned}$$

where $c = 2N_A$ is a constant, and $\frac{1}{N_A} \sum_{\mathbf{a}'} \mathbb{P}_{\hat{Y}|do(\mathbf{a}'), do(\mathbf{x}^{ad})}$ is the mixture distribution corresponding to the barycenter of distributions $\{\mathbb{P}(\hat{Y}|do(\mathbf{a}), do(\mathbf{x}^{ad}))\}_{\mathbf{a}}$. The equality holds from the fact that the MMD is a distance metric in the inner product space, called the reproducing kernel Hilbert space (RKHS); see Section B.1 for the derivation.

Second, we decrease the time for computing each MMD from $\mathcal{O}(n^2)$ to $\mathcal{O}(nd_{\text{RFF}})$ by approximating feature mapping $\phi(\cdot)$ of kernel function $k(\mathbf{y}, \mathbf{y}') = \langle \phi(\mathbf{y}), \phi(\mathbf{y}') \rangle$ as a d_{RFF} -dimensional vector of random Fourier features (RFFs) [Rahimi and Recht, 2007]. The MMD in (7) is defined as the distance in the RKHS \mathcal{H}_k between *kernel mean embeddings*:

$$\|\mu_{\hat{Y}|do(\mathbf{a}), do(\mathbf{x}^{ad})} - \mu_{\hat{Y}|do(\mathbf{a}'), do(\mathbf{x}^{ad})}\|_{\mathcal{H}_k}, \quad (8)$$

where kernel mean embedding $\mu_{\hat{Y}|do(\mathbf{a}), do(\mathbf{x}^{ad})}$ is defined as

$$\mu_{\hat{Y}|do(\mathbf{a}), do(\mathbf{x}^{ad})} := \mathbb{E}_{\hat{Y}|do(\mathbf{A}=\mathbf{a}), do(\mathbf{X}^{ad}=\mathbf{x}^{ad})}[\phi(\hat{Y})]. \quad (9)$$

RFFs approximate feature mapping $\phi(\cdot)$ in (9) as a vector:

$$\phi_{\text{RFF}}(\mathbf{y}) = [\cos(\omega_1^\top \mathbf{y} + b_1), \dots, \cos(\omega_{d_{\text{RFF}}}^\top \mathbf{y} + b_{d_{\text{RFF}}})]^\top,$$

where $\{\omega_i\}_{i=1}^{d_{\text{RFF}}}$ and $\{b_i\}_{i=1}^{d_{\text{RFF}}}$ are randomly sampled coefficients; with the Gaussian kernel k with bandwidth $\gamma > 0$, they are sampled from the Gaussian distribution $\mathcal{N}(0, \gamma^{-2})$ and the uniform distribution $\mathcal{U}[0, 2\pi]$, respectively.

With these two strategies, we can efficiently compute the worst-case MMD with $\mathcal{O}(MN_A N_{\mathbf{x}^{ad}} nd_{\text{RFF}})$.

3.3.2 Penalty Function Formulation

To estimate the barycenter MMD in (7), we develop a weighted estimator of the kernel mean embedding in (9), by combining *inverse probability weighting* (IPW) and RFFs.

Recall that interventional distribution $\mathbb{P}(\hat{Y}|do(\mathbf{a}), do(\mathbf{x}^{ad}))$ is identified using a valid adjustment set \mathbf{Z} as the conditional expectation in (5). Using IPW, this can be estimated as

$$\begin{aligned} & \mathbb{E}_{\mathbf{Z}, \mathbf{X}^{\text{re}} | \mathbf{a}, \mathbf{x}^{ad}} \left[\mathbb{P}(\hat{Y} = \hat{\mathbf{y}} | \mathbf{A} = \mathbf{a}, \mathbf{X}^{ad} = \mathbf{x}^{ad}, \mathbf{Z}, \mathbf{X}^{\text{re}}) \right], \\ & = \mathbb{E} \left[\frac{\mathbf{I}(\mathbf{a}, \mathbf{x}^{ad})}{\pi_{\mathbf{a}, \mathbf{x}^{ad}}(\mathbf{Z})} \mathbb{E}_{\mathbf{X}^{\text{re}} | \mathbf{A}, \mathbf{X}^{ad}, \mathbf{Z}} \left[\mathbb{P}(\hat{Y} = \hat{\mathbf{y}} | \mathbf{A}, \mathbf{X}^{ad}, \mathbf{Z}, \mathbf{X}^{\text{re}}) \right] \right], \quad (10) \end{aligned}$$

where $\mathbf{I}(\mathbf{a}, \mathbf{x}^{ad})$ is the indicator function that takes 1 if $\mathbf{A} = \mathbf{a}$ and $\mathbf{X}^{ad} = \mathbf{x}^{ad}$ for discrete $\mathbf{A}, \mathbf{X}^{ad}$; otherwise 0, $\pi_{\mathbf{a}, \mathbf{x}^{ad}}(\mathbf{Z}) := \mathbb{P}(\mathbf{A} = \mathbf{a}, \mathbf{X}^{ad} = \mathbf{x}^{ad} | \mathbf{Z})$ is the probability known as the *joint propensity score*, and $\mathbb{P}(\hat{Y} = \hat{\mathbf{y}} | \mathbf{a}, \mathbf{x}^{ad}, \mathbf{Z}, \mathbf{X}^{\text{re}})$ is the distribution of \hat{Y} given by predictive model h_θ . We derive Eqs. (5) and (10) in Section B.2.

As with (10), the kernel mean embedding in Eq. (9) can be estimated as an empirical weighted average of RFF vectors:

$$\hat{\mu}_{\hat{Y}|do(\mathbf{a}), do(\mathbf{x}^{ad})} = \frac{1}{n} \sum_{i=1}^n w_i \phi_{\text{RFF}}(\hat{\mathbf{y}}_i), \quad (11)$$

where $\hat{\mathbf{y}}_i = h_\theta(\mathbf{x}_i)$ is prediction, and w_i is an IPW weight:

$$w_i = \frac{\mathbf{I}(\mathbf{A}_i = \mathbf{a}, \mathbf{X}_i^{ad} = \mathbf{x}^{ad})}{\pi_{\mathbf{a}, \mathbf{x}^{ad}}(\mathbf{z}_i^m)}, \quad (12)$$

where $\pi_{\mathbf{a}, \mathbf{x}^{ad}}(\mathbf{z}_i^m) = \mathbb{P}(\mathbf{A} = \mathbf{a}, \mathbf{X}^{ad} = \mathbf{x}^{ad} | \mathbf{Z}^m = \mathbf{z}_i^m)$ is the joint propensity score computed by fitting $\pi_{\mathbf{a}, \mathbf{x}^{ad}}$ to the training data beforehand; we can apply IPW weight stabilization techniques like clipping/smoothing [Chikahara and Ushiyama, 2024], as empirically tested in Section E.6.

By computing the barycenter kernel MMD in (7) with weighted estimators (11), we obtain our penalty function as

$$\begin{aligned} & g_\theta(\mathbf{x}_1, \dots, \mathbf{x}_n) \\ & = \max_{m=1, \dots, M} \sum_{\mathbf{x}^{ad}} \sum_{\mathbf{a}} \|\hat{\mu}_{\hat{Y}|do(\mathbf{a}), do(\mathbf{x}^{ad})} - \hat{\mu}_{\hat{Y}|do(\mathbf{x}^{ad})}\|_2^2, \quad (13) \end{aligned}$$

where $\hat{\mu}_{\hat{Y}|do(\mathbf{x}^{ad})} = \frac{1}{N_A} \sum_{\mathbf{a}} \hat{\mu}_{\hat{Y}|do(\mathbf{a}), do(\mathbf{x}^{ad})}$ is the empirical barycenter. Since $\max_{m=1, \dots, M}$ is non-differentiable, we approximate it as the *Mellowmax* function [Asadi and Littman, 2017], empirically improving performance (Section E.6).

4 EXPERIMENTS

Baselines. We compare our cluster interventional fairness (**C-IFair**) method with six baselines. (i) **Full** uses all features without fairness constraints. (ii) **Unaware** uses all features except the sensitive features \mathbf{A} . (iii) **No-DesCs** uses all features except *definite descendant clusters* of \mathbf{A} (i.e., clusters that are descendants of \mathbf{A} in all cluster DAGs represented by the cluster CPDAG). (iv) ϵ -**IFair** [Zuo et al., 2024] penalizes the kernel MMD estimated using a variable-level CPDAG. (v) ℓ -**IFair** [Li et al., 2024] penalizes unfairness based on a local adjustment set search over a variable-level CPDAG. (vi) **Oracle** assumes access to the true variable-level DAG and uses all non-descendant *variables* of \mathbf{A} .

4.1 SYNTHETIC DATA EXPERIMENTS

Settings. We use linear and nonlinear synthetic datasets generated from variable-level causal DAGs. We randomly sample a causal DAG with $d_v = 3d$ variables (for each

Table 1: Root mean squared error (RMSE) and unfairness for linear (top) and nonlinear (bottom) datasets on test data

LINEAR	$d=5$ ($d_v=15$)		$d=10$ ($d_v=30$)		$d=15$ ($d_v=45$)	
	RMSE↓	UNFAIRNESS↓	RMSE↓	UNFAIRNESS↓	RMSE↓	UNFAIRNESS↓
ORACLE	0.957 ± 0.037	0.000 ± 0.000	0.977 ± 0.044	0.000 ± 0.000	1.069 ± 0.143	0.000 ± 0.000
FULL	0.523 ± 0.195	0.259 ± 0.129	0.483 ± 0.195	0.229 ± 0.136	0.554 ± 0.210	0.081 ± 0.117
UNAWARE	0.774 ± 0.154	0.071 ± 0.059	0.774 ± 0.154	0.062 ± 0.079	0.793 ± 0.120	0.046 ± 0.104
NO-DESCs	0.739 ± 0.140	0.064 ± 0.089	0.739 ± 0.140	0.065 ± 0.100	0.699 ± 0.135	0.033 ± 0.028
ϵ -IFAIR	0.647 ± 0.030	0.069 ± 0.031	0.663 ± 0.062	0.071 ± 0.011	0.671 ± 0.044	0.040 ± 0.011
ℓ -IFAIR	0.875 ± 0.028	0.069 ± 0.081	0.964 ± 0.049	0.072 ± 0.052	0.764 ± 0.049	0.052 ± 0.052
C-IFAIR	0.643 ± 0.127	0.060 ± 0.054	0.660 ± 0.123	0.056 ± 0.052	0.669 ± 0.171	0.020 ± 0.036

NONLINEAR	$d=5$ ($d_v=15$)		$d=10$ ($d_v=30$)		$d=15$ ($d_v=45$)	
	RMSE↓	UNFAIRNESS↓	RMSE↓	UNFAIRNESS↓	RMSE↓	UNFAIRNESS↓
ORACLE	1.008 ± 0.030	0.000 ± 0.000	1.055 ± 0.069	0.000 ± 0.000	1.000 ± 0.073	0.000 ± 0.000
FULL	0.914 ± 0.066	0.121 ± 0.073	0.925 ± 0.055	0.026 ± 0.026	0.928 ± 0.058	0.021 ± 0.007
UNAWARE	0.978 ± 0.058	0.069 ± 0.073	0.957 ± 0.061	0.027 ± 0.038	1.014 ± 0.055	0.024 ± 0.017
NO-DESCs	0.978 ± 0.061	0.084 ± 0.113	0.950 ± 0.066	0.022 ± 0.028	1.022 ± 0.069	0.020 ± 0.008
ϵ -IFAIR	0.938 ± 0.006	0.077 ± 0.009	0.953 ± 0.026	0.027 ± 0.000	0.962 ± 0.016	0.023 ± 0.001
ℓ -IFAIR	0.987 ± 0.065	0.076 ± 0.042	0.982 ± 0.041	0.023 ± 0.010	1.042 ± 0.041	0.017 ± 0.010
C-IFAIR	0.929 ± 0.051	0.066 ± 0.046	0.948 ± 0.051	0.021 ± 0.035	0.960 ± 0.036	0.010 ± 0.012

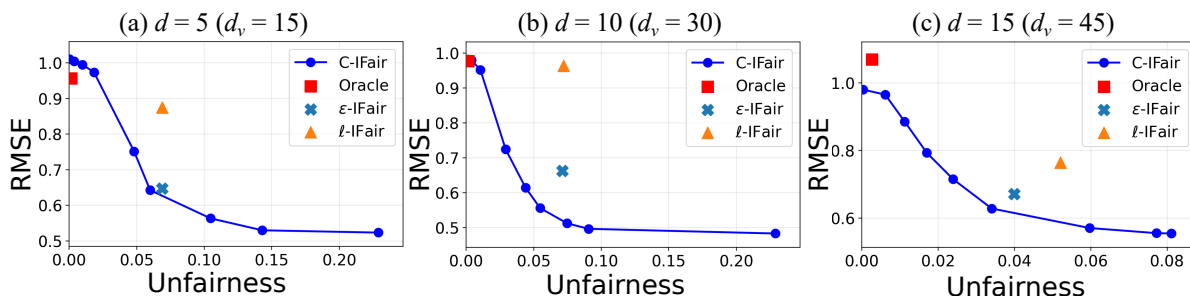


Figure 3: Performance on linear datasets when varying λ from 0 to 200: (a): $d = 5$, (b): $d = 10$, and (c): $d = 15$ clusters.

$d \in \{5, 10, 15\}$) from an Erdős–Rényi (ER) model with an expected degree of 2. Using the resulting DAGs and corresponding linear or nonlinear SCMs, we generate 20 datasets with sample size $n = 5000$, each of which is split into training (80%), validation (10%), and test (10%) sets.

By applying CLOC to each dataset, we infer a cluster CPDAG over d clusters, using a randomly generated partition with 3 variables per cluster. We then select one cluster consisting of binary variables as the sensitive cluster \mathbf{A} . In our main experiments, we set the admissible cluster \mathbf{X}^{ad} to be empty; results with \mathbf{X}^{ad} are provided in Section E.1.

To evaluate unfairness, we estimate the MMD on the test set by sampling interventional datasets with the true SCM.

Performance Comparison. Table 1 reports the mean and standard deviation of RMSE and unfairness over 20 datasets.

Among the baselines (excluding **Oracle** and **Full**), our **C-IFair** performs best in both RMSE and unfairness across all settings, highlighting the effectiveness of our cluster-

graph-based framework. While maintaining high accuracy, it achieves fairness closest to **Oracle**, which requires the true variable-level DAG—an unrealistic requirement in practice.

Unaware and **No-DesCs** exhibit high RMSE and unfairness, implying that discarding potentially predictive features is insufficient to remove indirect effects due to graph uncertainty. ϵ -**IFair** and ℓ -**IFair** produce less fair predictions than our **C-IFair** in high-dimensional setups ($d = 15$), indicating that inferred variable-level CPDAGs can be unreliable in such setups. We provide supporting evidence for this claim in Section E.5 in comparison with cluster CPDAG inference, following the procedure of Anand et al. [2025].

Accuracy–Fairness Trade-Off. To assess the effect of penalty function g_θ , we vary the parameter λ from 0 to 200.

Figure 3 shows results on the linear datasets. As expected, increasing λ reduces unfairness at the cost of higher RMSE, demonstrating that **C-IFair** can flexibly control the trade-off by tuning λ to meet application-specific requirements.

Table 2: Area Under the Curve (AUC) and unfairness for real-world datasets on the held-out test set using 20 random seeds

	ADULT		GERMAN		OULAD	
	AUC \uparrow	UNFAIRNESS \downarrow	AUC \uparrow	UNFAIRNESS \downarrow	AUC \uparrow	UNFAIRNESS \downarrow
ORACLE	0.709 \pm 0.009	0.000 \pm 0.000	0.582 \pm 0.004	0.000 \pm 0.000	0.628 \pm 0.015	0.000 \pm 0.000
FULL	0.874 \pm 0.004	0.030 \pm 0.024	0.762 \pm 0.060	0.173 \pm 0.011	0.697 \pm 0.024	0.061 \pm 0.001
UNAWARE	0.805 \pm 0.049	0.018 \pm 0.014	0.695 \pm 0.061	0.101 \pm 0.013	0.654 \pm 0.019	0.004 \pm 0.000
NO-DESCS	0.815 \pm 0.007	0.026 \pm 0.022	0.726 \pm 0.059	0.085 \pm 0.008	0.654 \pm 0.020	0.004 \pm 0.000
ϵ -IFAIR	0.812 \pm 0.006	0.015 \pm 0.012	0.756 \pm 0.008	0.082 \pm 0.000	0.641 \pm 0.005	0.005 \pm 0.002
ℓ -IFAIR	0.764 \pm 0.002	0.015 \pm 0.008	0.750 \pm 0.035	0.151 \pm 0.011	0.639 \pm 0.011	0.003 \pm 0.001
C-IFAIR	0.829 \pm 0.021	0.014 \pm 0.010	0.760 \pm 0.061	0.065 \pm 0.008	0.660 \pm 0.018	0.001 \pm 0.000

4.2 REAL-WORLD DATA EXPERIMENTS

Settings. We use three standard benchmarks, the Adult, German credit, and OULAD datasets. To evaluate unfairness in the absence of ground-truth SCMs, we compute the weighted MMD estimator in (7) by leveraging the variable-level DAGs used in prior works (Section D.4).

Performance Comparison. Table 2 presents the AUC and unfairness on the three datasets. Again, our **C-IFair** achieves the best performance in terms of both AUC and unfairness among all baselines (except **Oracle** and **Full**), thus underscoring its practical utility for real-world applications.

Fairness Illustration. We compare the inferred interventional distributions over prediction $\hat{Y} \in \{0, 1\}$ on the Adult dataset. Following Zuo et al. [2024], we estimate probability $P(\hat{Y} = 1 \mid do(A = \mathbf{a}))$ for different values \mathbf{a} by approximating the SCM via conditional density estimation.

Figure 4 shows the probability difference from baseline value $\mathbf{a} = [0, 0]$. Our **C-IFair** makes sufficiently fair predictions with respect to sensitive features A (gender and race), thus highlighting its effectiveness in practical applications.

4.3 ADDITIONAL EXPERIMENTS

Results in Section E support the following key findings:

- **In presence of admissible clusters:** Our **C-IFair** performs best in these challenging setups (Section E.1).
- **Dense graphs:** Despite the change in number of adjustment sets M , our **C-IFair** works best (Section E.2).
- **Inadmissible partitions:** Empirically, the inferred graphs can still enforce fairness (Section E.3).

5 RELATED WORK

Achieving fairness under causal graph uncertainty has been a long-standing challenge. Prior work has addressed counterfactual fairness using manually designed candidate graphs

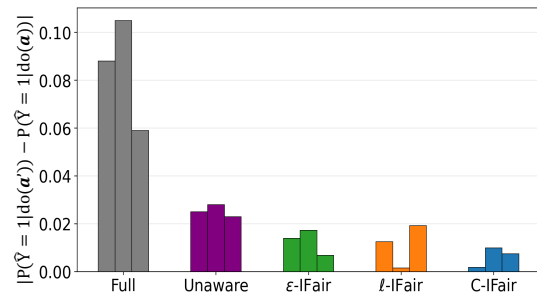


Figure 4: Probability difference between intervened values $\mathbf{a}' = [0, 1], [1, 0], [1, 1]$ and $\mathbf{a} = [0, 0]$ on Adult dataset

[Russell et al., 2017, Chikahara et al., 2023]. ϵ -IFair [Zuo et al., 2024] was the first to leverage a CPDAG, but it assumes that no feature is connected to a sensitive feature via an undirected edge. ℓ -IFair [Li et al., 2024] relaxes this assumption, yet it still requires accurate CPDAG estimation.

Our **C-IFair** advances this line of work by providing a principled framework for leveraging cluster-level causal structure, which can be reliably inferred from the data.

6 CONCLUSION

We propose a learning framework for achieving interventional fairness from the cluster CPDAG structure, whose inference requires substantially fewer conditional independence tests than the variable-level CPDAG. To overcome the identification challenges in cluster CPDAGs, we establish a graphical algorithm for identifying valid adjustment sets. By computing the maximum MMD over these sets, we enforce interventional fairness in the presence of graph uncertainty.

A promising direction for future work is to extend our framework to incorporate additional domain knowledge about the graph structure, just as the extension of CPDAG-based methods to maximally oriented partial directed acyclic graphs (MPDAGs) [Li et al., 2024, Zuo et al., 2024]. Although extending cluster CPDAGs to cluster MPDAGs is highly non-trivial, it would further reduce the uncertainty in causal structures and improve the fairness-accuracy trade-off.

Acknowledgements

This work was supported by JST ACT-X (JPMJAX23CF).

References

- Tara V. Anand, Adele H. Ribeiro, Jin Tian, and Elias Bareinboim. Causal effect identification in cluster DAGs. In *AAAI*, volume 37, pages 12172–12179, 2023.
- Tara Vafai Anand, Adèle H. Ribeiro, Jin Tian, George Hripcsak, and Elias Bareinboim. Causal discovery over clusters of variables in Markovian systems. In *NeurIPS*, 2025.
- Kavosh Asadi and Michael L. Littman. An alternative softmax operator for reinforcement learning. In *ICML*, pages 243–252, 2017.
- K. Bache and M. Lichman. UCI machine learning repository: Datasets. <http://archive.ics.uci.edu/ml/datasets>, 2013.
- Silvia Chiappa and Thomas P. S. Gillam. Path-specific counterfactual fairness. In *AAAI*, pages 7801–7808, 2019.
- David Maxwell Chickering. Learning equivalence classes of Bayesian-network structures. *JMLR*, 2:445–498, 2002.
- Yoichi Chikahara and Kansei Ushiyama. Differentiable Pareto-smoothed weighting for high-dimensional heterogeneous treatment effect estimation. In *UAI*, pages 749–762, 2024.
- Yoichi Chikahara, Shinsaku Sakaue, Akinori Fujino, and Hisashi Kashima. Learning individually fair classifier with path-specific causal-effect constraint. In *AISTATS*, pages 145–153, 2021.
- Yoichi Chikahara, Shinsaku Sakaue, Akinori Fujino, and Hisashi Kashima. Making individually fair predictions with causal pathways. *Data Mining and Knowledge Discovery*, 37(4):1327–1373, 2023.
- Zhuangyan Fang and Yangbo He. IDA with background knowledge. In *UAI*, pages 270–279, 2020.
- Andreas Fuster, Paul Goldsmith-Pinkham, Tarun Ramadorai, and Ansgar Walther. Predictably unequal? the effects of machine learning on credit markets. *Journal of Finance*, 77(1):5–47, 2022.
- Clark Glymour, Kun Zhang, and Peter Spirtes. Review of causal discovery methods based on graphical models. *Frontiers in Genetics*, 10:524, 2019.
- Arthur Gretton, Karsten M. Borgwardt, Malte J. Rasch, Bernhard Schölkopf, and Alexander Smola. A kernel two-sample test. *JMLR*, 13(1):723–773, 2012.
- F. Richard Guo and Emilija Perković. Efficient least squares for estimating total effects under linearity and causal sufficiency. *JMLR*, 23(104):1–41, 2022.
- Kimberly A. Houser. Can AI solve the diversity problem in the tech industry: Mitigating noise and bias in employment decision-making. *Stanford Technology Law Review*, 22:290, 2019.
- Woojin Kim and Hyeoncheol Kim. Counterfactual fairness evaluation of machine learning models on educational datasets. In *International Conference on Intelligent Tutoring Systems*, pages 88–103, 2025.
- Matt J. Kusner, Joshua Loftus, Chris Russell, and Ricardo Silva. Counterfactual fairness. In *NeurIPS*, pages 4066–4076, 2017.
- Haoxuan Li, Yue Liu, Zhi Geng, and Kun Zhang. A local method for satisfying interventional fairness with partially known causal graphs. In *NeurIPS*, pages 135415–135436, 2024.
- Ilya Loshchilov and Frank Hutter. Decoupled weight decay regularization. In *ICLR*, 2019.
- Marloes H. Maathuis, Markus Kalisch, and Peter Bühlmann. Estimating high-dimensional intervention effects from observational data. *Annals of Statistics*, 37(6A):3133, 2009.
- Judea Pearl. *Causality: Models, Reasoning and Inference*. Cambridge University Press, 2009.
- Emilija Perkovic. Identifying causal effects in maximally oriented partially directed acyclic graphs. In *UAI*, pages 530–539, 2020.
- Ali Rahimi and Benjamin Recht. Random features for large-scale kernel machines. In *NeurIPS*, pages 1177–1184, 2007.
- Joseph D. Ramsey, Kun Zhang, Madelyn Glymour, Ruben Sanchez Romero, Biwei Huang, Imme Ebert-Uphoff, Savini Samarasinghe, Elizabeth A. Barnes, and Clark Glymour. TETRAD—a toolbox for causal discovery. In *International Workshop on Climate Informatics*, pages 1–4, 2018.
- Chris Russell, Matt J. Kusner, Joshua Loftus, and Ricardo Silva. When worlds collide: Integrating different counterfactual assumptions in fairness. In *NeurIPS*, pages 6414–6423, 2017.
- Babak Salimi, Luke Rodriguez, Bill Howe, and Dan Suciu. Interventional fairness: Causal database repair for algorithmic fairness. In *SIGMOD*, pages 793–810, 2019.
- Eran Segal, Dana Pe’er, Aviv Regev, Daphne Koller, Nir Friedman, and Tommi Jaakkola. Learning module networks. *JMLR*, 6(4), 2005.

- Peter Spirtes, Clark N. Glymour, Richard Scheines, David Heckerman, Christopher Meek, Gregory Cooper, and Thomas Richardson. *Causation, prediction, and search*. MIT press, 2000.
- Santtu Tikka, Jouni Helske, and Juha Karvanen. Clustering and structural robustness in causal diagrams. *JMLR*, 24 (195):1–32, 2023.
- Jonas Wahl, Urmi Ninad, and Jakob Runge. Foundations of causal discovery on groups of variables. *Journal of Causal Inference*, 12(1):20230041, 2024.
- David S. Watson, Limor Gultchin, Ankur Taly, and Luciano Floridi. Local explanations via necessity and sufficiency: Unifying theory and practice. In *UAI*, pages 1382–1392, 2021.
- Yongkai Wu, Lu Zhang, Xintao Wu, and Hanghang Tong. PC-fairness: A unified framework for measuring causality-based fairness. In *NeurIPS*, pages 3399–3409, 2019.
- Lu Zhang, Yongkai Wu, and Xintao Wu. Achieving non-discrimination in data release. In *KDD*, pages 1335–1344, 2017.
- Yujia Zheng, Biwei Huang, Wei Chen, Joseph Ramsey, Mingming Gong, Ruichu Cai, Shohei Shimizu, Peter Spirtes, and Kun Zhang. Causal-learn: Causal discovery in Python. *JMLR*, 25(60):1–8, 2024.
- Aoqi Zuo, Yiqing Li, Susan Wei, and Mingming Gong. Interventional fairness on partially known causal graphs: A constrained optimization approach. In *ICLR*, 2024.

Fairness under Graph Uncertainty: Achieving Interventional Fairness with Partially Known Causal Graphs over Clusters of Variables (Supplementary Material)

Yoichi Chikahara¹

¹NTT Communication Science Laboratories, Kyoto, Japan

A BACKGROUND ON CLUSTER CAUSAL GRAPHS

A.1 NOTIONS FOR VARIABLE-LEVEL GRAPHS

We first present some graphical notions used in this paper.

Variable-level d-separation. A triplet of nodes $\langle V_i, V_k, V_j \rangle$ in a variable-level DAG G_v is *active* relative to a set of nodes \mathbf{Z} if either (i) V_k is a collider or any of its descendants are in \mathbf{Z} , or (ii) V_k is a non-collider and $V_k \notin \mathbf{Z}$. A path p is *active* given \mathbf{Z} if every triplet on p is active relative to \mathbf{Z} . Otherwise, p is *inactive*. Given a variable-level causal DAG G_v , two node sets \mathbf{X} and \mathbf{Y} are *d-separated* by a set of nodes \mathbf{Z} , if there is no active path between \mathbf{X} and \mathbf{Y} given \mathbf{Z} . We denote d-separation in a variable-level causal DAG G_v by $(\mathbf{X}, \mathbf{Y} \mid \mathbf{Z})_{G_v}$.

Definite Colliders and Definite Non-Colliders in Variable-level CPDAGs. A variable-level CPDAG has directed and undirected edges, where directed edges are common to all DAGs represented by the CPDAG, while undirected edges indicate uncertainty in edge directions in the DAGs. A *definite collider* and a *definite non-collider* are a collider and a non-collider in all DAGs represented by the variable-level CPDAG, respectively. They are determined for each *shielded* triplet $\langle X, Z, Y \rangle$ (i.e., a triplet where nodes X and Y are adjacent to each other) and each *unshielded* triplet $\langle X, Z, Y \rangle$ (i.e., a triplet where nodes X and Y are non-adjacent to each other). Z in a triplet $\langle X, Z, Y \rangle$ is a definite collider if $X \rightarrow Z \leftarrow Y$ in the CPDAG. Z is a definite non-collider if either (i) at least one edge is out of it (i.e., $X \leftarrow Z - Y$ or $X - Z \rightarrow Y$), or (ii) both edges are undirected ($X - Z - Y$) and the triplet is unshielded.

A.2 DEFINITION OF CLUSTER CAUSAL GRAPHS

We present a brief overview of the definition of cluster causal graphs based on Anand et al. [2025].

Independence arcs. Independence arcs describe the conditional independence relationships in an unshielded triplet of clusters $\langle C_i, C_k, C_j \rangle$ in a cluster DAG. For a shielded triplet $\langle C_i, C_k, C_j \rangle$, we consider the unshielded triplet formed by removing the edge between C_i and C_j , which is referred to as a *manipulated unshielded triplet* in Anand et al. [2025].

Definition A.1 (Independence arcs [Anand et al., 2025]). For any unshielded triplet (and any manipulated unshielded triplet) of clusters $\langle C_i, C_k, C_j \rangle$ in a cluster DAG G over clusters $\mathcal{C} = \{C_1, \dots, C_m\}$, let S be a (possibly empty) set of clusters

$$S \subseteq \mathcal{C} \setminus \{C_i, C_j\} \quad \text{such that} \quad C_i \perp C_j \mid S,$$

if at least one such separating set exists (if multiple exist, fix any one of them).

Define the independence arc $\mathcal{A}_{\langle C_i, C_k, C_j \rangle}$ (drawn between the two edges incident to C_k in the triplet) by:

1. $\mathcal{A}_{\langle C_i, C_k, C_j \rangle} = \text{marg}$ if and only if $C_k \in S$.

2. $\mathcal{A}_{\langle \mathbf{C}_i, \mathbf{C}_k, \mathbf{C}_j \rangle} = \text{cond}$ if and only if $\mathbf{C}_k \notin S$ and $\mathbf{C}_i \not\perp \mathbf{C}_j \mid (S \cup \{\mathbf{C}_k\})$.
3. $\mathcal{A}_{\langle \mathbf{C}_i, \mathbf{C}_k, \mathbf{C}_j \rangle} = \text{never}$ if and only if $\mathbf{C}_k \notin S$ and $\mathbf{C}_i \perp \mathbf{C}_j \mid (S \cup \{\mathbf{C}_k\})$.

Separation and Connection Marks. Separation and connection marks annotate independence arcs with marg and cond and those with never, respectively, to indicate the exceptional cases where the corresponding conditional independence relationships do not hold.

Formally, separation marks are defined as follows.

Definition A.2 (Separation marks [Anand et al., 2025]). Let G_v be a variable-level DAG and G be a cluster DAG with independence arcs as in Definition A.1. Consider a cluster path

$$p_c = \langle \mathbf{C}_1, \mathbf{C}_2, \dots, \mathbf{C}_n \rangle \quad (n \geq 4)$$

and its arc trajectory

$$a = \langle \mathcal{A}_{\langle \mathbf{C}_1, \mathbf{C}_2, \mathbf{C}_3 \rangle}, \mathcal{A}_{\langle \mathbf{C}_2, \mathbf{C}_3, \mathbf{C}_4 \rangle}, \dots, \mathcal{A}_{\langle \mathbf{C}_{n-2}, \mathbf{C}_{n-1}, \mathbf{C}_n \rangle} \rangle.$$

Assume:

1. no arc in a is of type never;
2. there exists *no* d-connecting variable-level path in G_v (relative to some set of clusters) that is analogous to p_c ;
3. there exists a d-connecting variable-level path (relative to some set of clusters) analogous to the prefix path $\langle \mathbf{C}_1, \dots, \mathbf{C}_{n-1} \rangle$;
4. there exists a d-connecting variable-level path (relative to some set of clusters) analogous to the suffix path $\langle \mathbf{C}_2, \dots, \mathbf{C}_n \rangle$.

Then we place a *separation mark* $\circlearrowleft_{\mathbf{C}_1}$ on the last arc $\mathcal{A}_{\langle \mathbf{C}_{n-2}, \mathbf{C}_{n-1}, \mathbf{C}_n \rangle}$, and symmetrically place $\circlearrowright_{\mathbf{C}_n}$ on the first arc $\mathcal{A}_{\langle \mathbf{C}_1, \mathbf{C}_2, \mathbf{C}_3 \rangle}$.

In Definition A.2, the concept of *analogous paths* is used, which is defined as follows.

Definition A.3 (Analogous paths [Anand et al., 2025]). Let G_v be a variable-level DAG, and let G be a cluster DAG over clusters $\mathcal{C} = \{\mathbf{C}_1, \dots, \mathbf{C}_d\}$, where each cluster \mathbf{C} contains a set of variables in G_v . Consider a path over clusters

$$p_c = \langle \mathbf{C}_1, \mathbf{C}_2, \dots, \mathbf{C}_n \rangle$$

in G , and a path over variables

$$p_v = \langle V_1, V_2, \dots, V_m \rangle$$

in G_v . We say that p_v is *analogous* to p_c (and vice versa) if and only if:

1. every variable on p_v belongs to one of the clusters appearing on p_c ;
2. every cluster appearing on p_c contributes at least one variable to p_v ;
3. the order along p_v is consistent with the order of clusters along p_c in the sense that, once p_v visits some variable in the last cluster \mathbf{C}_t (for any t), it never later visits a variable that lies in any earlier cluster \mathbf{C}_s with $s < t$ ($s, t \in \{1, \dots, n\}$).

By contrast, connection marks are defined as follows.

Definition A.4 (Connection marks [Anand et al., 2025]). Let G_v be a variable-level DAG and G be a cluster DAG with independence arcs. Consider a triplet of clusters $\langle \mathbf{C}_i, \mathbf{C}_k, \mathbf{C}_j \rangle$ in G and its independence arc $\mathcal{A}_{\langle \mathbf{C}_i, \mathbf{C}_k, \mathbf{C}_j \rangle}$. Assume that $\mathcal{A}_{\langle \mathbf{C}_i, \mathbf{C}_k, \mathbf{C}_j \rangle} \in \{\text{never}, \text{cond}\}$.

If there exists a variable-level path in G_v that passes through variables

$$\langle V_i, \dots, V_k, \dots, V_j \rangle \quad \text{with } V_i \in \mathbf{C}_i, V_k \in \mathbf{C}_k, V_j \in \mathbf{C}_j,$$

then for each collider variable $V'_k \in \mathbf{C}_k$ that lies on such a path, collect the clusters that contain *children* (equivalently, descendants via one outgoing step) of that collider along the same path:

$$D = \bigcup \{ \mathbf{C}_d \in \mathcal{C} \setminus \{ \mathbf{C}_i, \mathbf{C}_k, \mathbf{C}_j \} : \exists V_d \in \mathbf{C}_d \text{ with } V_d \in \text{Ch}(V'_k) \}.$$

We then add the *connection mark* \oplus_D to the independence arc $\mathcal{A}_{\langle \mathbf{C}_i, \mathbf{C}_k, \mathbf{C}_j \rangle}$.

Cluster Causal DAG with Independence Arcs. Using the notions of independence arcs, separation marks, and connection marks, cluster causal DAGs with independence arcs are defined as follows.

Definition A.5 (Cluster Causal DAGs [Anand et al., 2025]). Given a variable-level DAG G_v and an admissible partition of clusters $\mathcal{C} = \{\mathcal{C}_1, \dots, \mathcal{C}_d\}$ of variables in G_v , a *cluster causal DAG with independence arcs* is defined as a DAG $G = (\mathcal{C}, \mathcal{E}, \mathcal{A})$ over clusters \mathcal{C} such that

- An edge $\mathcal{C}_i \rightarrow \mathcal{C}_j$ is in \mathcal{E} if there exist some $V_i \in \mathcal{C}_i$ and $V_j \in \mathcal{C}_j$ such that $V_i \rightarrow V_j$ is in G_v ;
- The set of independence arcs \mathcal{A} is defined according to Definition A.1;
- The separation marks and connection marks are defined according to Definition A.2 and Definition A.4, respectively.

Cluster CPDAGs. A cluster CPDAG with independence arcs is defined as the equivalence class of cluster causal DAGs with independence arcs that entail the same set of conditional independence relationships over clusters.

Definition A.6 (Cluster CPDAGs [Anand et al., 2025]). Let $[G]$ be the cluster MEC of a cluster causal DAG G over clusters $\mathcal{C} = \{\mathcal{C}_1, \dots, \mathcal{C}_d\}$. The *cluster CPDAG with independence arcs* for the cluster MEC $[G]$, denoted by \mathcal{G} , is defined such that

- \mathcal{G} has the same skeleton as G and its any member of $[G]$;
- A directed edge is present in \mathcal{G} if it is present in all members of $[G]$; otherwise, the edge is undirected;
- An independence arc is present in \mathcal{G} if it is present in all members of $[G]$; otherwise, the independence arc is absent;
- \mathcal{G} has the same separation marks and connection marks as G and its any member of $[G]$.

A.3 ASSUMPTION ON CLUSTER CAUSAL GRAPHS

The CLOC algorithm [Anand et al., 2025] for learning cluster CPDAGs from data relies on the faithfulness assumption at the cluster level (Assumption 3.3), which is defined as follows.

Definition A.7 (Cluster-level Faithfulness [Anand et al., 2025]). Let G be a cluster DAG G over clusters \mathcal{C} , and let $P(\mathcal{C})$ be the joint distribution $P(\mathcal{C})$ over \mathcal{C} that is generated from an SCM compatible with a causal DAG G_v compatible with G . Then $P(\mathcal{C})$ is *faithful* to G if conditional independence relationships across clusters \mathcal{C} imply the cluster-level d-separation (Definition 3.4) in G ; that is, for any disjoint cluster sets $\mathbf{X}, \mathbf{Y}, \mathbf{Z} \subseteq \mathcal{C}$,

$$(\mathbf{X} \perp\!\!\!\perp \mathbf{Y} \mid \mathbf{Z})_{P(\mathcal{C})} \implies (\mathbf{X}, \mathbf{Y} \mid \mathbf{Z})_G.$$

B DERIVATIONS

In this section, we provide the detailed derivations of the equations presented in the main paper.

B.1 BARYCENTER KERNEL MMD (EQ. (7))

In Eq. (7), we decompose the summation of kernel MMDs over sensitive feature value pairs $(\mathbf{a}, \mathbf{a}')$ into the sum of barycenter MMDs. We drop the subscript m for adjustment set \mathbf{Z}_m for notational simplicity and restate Eq. (7) as

$$\sum_{\mathbf{a}, \mathbf{a}'} \text{MMD} \left(P_{\hat{Y}|do(\mathbf{a}), do(\mathbf{x}^{ad})}, P_{\hat{Y}|do(\mathbf{a}'), do(\mathbf{x}^{ad})} \right) = 2N_A \sum_{\mathbf{a}} \text{MMD} \left(P_{\hat{Y}|do(\mathbf{a}), do(\mathbf{x}^{ad})}, \frac{1}{N_A} \sum_{\mathbf{a}'} P_{\hat{Y}|do(\mathbf{a}'), do(\mathbf{x}^{ad})} \right).$$

Derivation. Fix \mathbf{x}^{ad} and define $P_a := P_{\hat{Y}|do(a), do(\mathbf{x}^{\text{ad}})}$. Let \mathcal{H} be the RKHS associated with the kernel and feature map $\phi : \text{supp}(\hat{Y}) \rightarrow \mathcal{H}$, and define the kernel mean embedding

$$\mu_a := \mathbb{E}_{\hat{Y} \sim P_a} [\phi(\hat{Y})] \in \mathcal{H}.$$

We use the (squared) RKHS distance representation of the kernel MMD:

$$\text{MMD}(P, Q) = \|\mu_P - \mu_Q\|_{\mathcal{H}}^2.$$

Then

$$\sum_{a, a'} \text{MMD}(P_a, P_{a'}) = \sum_{a, a'} \|\mu_a - \mu_{a'}\|_{\mathcal{H}}^2.$$

Expanding the squared norm gives

$$\sum_{a, a'} \|\mu_a - \mu_{a'}\|_{\mathcal{H}}^2 = \sum_{a, a'} \left(\|\mu_a\|_{\mathcal{H}}^2 + \|\mu_{a'}\|_{\mathcal{H}}^2 - 2\langle \mu_a, \mu_{a'} \rangle_{\mathcal{H}} \right) = 2N_A \sum_a \|\mu_a\|_{\mathcal{H}}^2 - 2 \left\| \sum_a \mu_a \right\|_{\mathcal{H}}^2.$$

Now define the barycenter (mixture) distribution

$$\bar{P} := \frac{1}{N_A} \sum_{a'} P_{a'}.$$

By linearity of expectation, its kernel mean embedding is

$$\bar{\mu} := \mu_{\bar{P}} = \mathbb{E}_{\hat{Y} \sim \bar{P}} [\phi(\hat{Y})] = \frac{1}{N_A} \sum_{a'} \mu_{a'}.$$

Expanding the squared norm with $\bar{\mu}$ yields

$$\sum_a \|\mu_a - \bar{\mu}\|_{\mathcal{H}}^2 = \sum_a \left(\|\mu_a\|_{\mathcal{H}}^2 - 2\langle \mu_a, \bar{\mu} \rangle_{\mathcal{H}} + \|\bar{\mu}\|_{\mathcal{H}}^2 \right) = \sum_a \|\mu_a\|_{\mathcal{H}}^2 - 2 \left\langle \sum_a \mu_a, \bar{\mu} \right\rangle_{\mathcal{H}} + N_A \|\bar{\mu}\|_{\mathcal{H}}^2.$$

Since the inner product is given by

$$\left\langle \sum_a \mu_a, \bar{\mu} \right\rangle_{\mathcal{H}} = \left\langle \sum_a \mu_a, \frac{1}{N_A} \sum_{a'} \mu_{a'} \right\rangle_{\mathcal{H}} = \frac{1}{N_A} \left\| \sum_a \mu_a \right\|_{\mathcal{H}}^2 = N_A \|\bar{\mu}\|_{\mathcal{H}}^2,$$

the sum of squared norms simplifies to

$$\sum_a \|\mu_a - \bar{\mu}\|_{\mathcal{H}}^2 = \sum_a \|\mu_a\|_{\mathcal{H}}^2 - 2N_A \|\bar{\mu}\|_{\mathcal{H}}^2 + N_A \|\bar{\mu}\|_{\mathcal{H}}^2 = \sum_a \|\mu_a\|_{\mathcal{H}}^2 - N_A \|\bar{\mu}\|_{\mathcal{H}}^2.$$

Hence we have

$$\sum_{a, a'} \|\mu_a - \mu_{a'}\|_{\mathcal{H}}^2 = 2N_A \sum_a \|\mu_a\|_{\mathcal{H}}^2 - 2N_A^2 \|\bar{\mu}\|_{\mathcal{H}}^2 = 2N_A \sum_a \|\mu_a - \bar{\mu}\|_{\mathcal{H}}^2,$$

Finally, since $\|\mu_a - \bar{\mu}\|_{\mathcal{H}}^2 = \text{MMD}(P_a, \bar{P})$, we obtain

$$\sum_{a, a'} \text{MMD}(P_a, P_{a'}) = 2N_A \sum_a \text{MMD}\left(P_a, \frac{1}{N_A} \sum_{a'} P_{a'}\right),$$

which is Eq. (7).

B.2 IDENTIFICATION AND ESTIMATION OF INTERVENTIONAL DISTRIBUTIONS (EQS. (5) AND (10))

We first restate Eqs. (5) and (10) below.

$$\begin{aligned} P(\hat{Y} = \hat{y} \mid do(\mathbf{A} = \mathbf{a}), do(\mathbf{X}^{\text{ad}} = \mathbf{x}^{\text{ad}})) &= \mathbb{E}_{\mathbf{Z}, \mathbf{X}^{\text{re}} \mid \mathbf{a}, \mathbf{x}^{\text{ad}}} \left[P(\hat{Y} = \hat{y} \mid \mathbf{A} = \mathbf{a}, \mathbf{X}^{\text{ad}} = \mathbf{x}^{\text{ad}}, \mathbf{Z}, \mathbf{X}^{\text{re}}) \right] \\ &= \mathbb{E} \left[\frac{\mathbf{I}(\mathbf{a}, \mathbf{x}^{\text{ad}})}{\pi_{\mathbf{a}, \mathbf{x}^{\text{ad}}}(\mathbf{Z})} \mathbb{E}_{\mathbf{X}^{\text{re}} \mid \mathbf{A}, \mathbf{X}^{\text{ad}}, \mathbf{Z}} \left[P(\hat{Y} = \hat{y} \mid \mathbf{A}, \mathbf{X}^{\text{ad}}, \mathbf{Z}, \mathbf{X}^{\text{re}}) \right] \right]. \end{aligned}$$

Below we provide the derivation of these equations.

Derivation. We derive Eq. (5) and Eq. (10) from the observed distribution. Let \mathbf{Z} be a valid adjustment set, and let \mathbf{X}^{re} denote the remaining features except \mathbf{A} , \mathbf{X}^{ad} , and \mathbf{Z} .

Step 1 (Eq. (5)). By marginalizing out \mathbf{Z} and \mathbf{X}^{re} under the intervention, we obtain

$$\begin{aligned} &P(\hat{Y} = \hat{y} \mid do(\mathbf{A} = \mathbf{a}), do(\mathbf{X}^{\text{ad}} = \mathbf{x}^{\text{ad}})) \\ &= \sum_{\mathbf{z}} \sum_{\mathbf{x}^{\text{re}}} P(\hat{Y} = \hat{y} \mid \mathbf{A} = \mathbf{a}, \mathbf{X}^{\text{ad}} = \mathbf{x}^{\text{ad}}, \mathbf{Z} = \mathbf{z}, \mathbf{X}^{\text{re}} = \mathbf{x}^{\text{re}}) P(\mathbf{X}^{\text{re}} = \mathbf{x}^{\text{re}} \mid \mathbf{A} = \mathbf{a}, \mathbf{X}^{\text{ad}} = \mathbf{x}^{\text{ad}}, \mathbf{Z} = \mathbf{z}) P(\mathbf{Z} = \mathbf{z}) \\ &= \mathbb{E}_{\mathbf{Z}} \left[\mathbb{E}_{\mathbf{X}^{\text{re}} \mid \mathbf{A} = \mathbf{a}, \mathbf{X}^{\text{ad}} = \mathbf{x}^{\text{ad}}, \mathbf{Z}} \left[P(\hat{Y} = \hat{y} \mid \mathbf{A} = \mathbf{a}, \mathbf{X}^{\text{ad}} = \mathbf{x}^{\text{ad}}, \mathbf{Z}, \mathbf{X}^{\text{re}}) \right] \right]. \end{aligned} \quad (14)$$

Step 2 (Eq. (10)). Define the joint propensity score by

$$\pi_{\mathbf{a}, \mathbf{x}^{\text{ad}}}(\mathbf{Z}) := P(\mathbf{A} = \mathbf{a}, \mathbf{X}^{\text{ad}} = \mathbf{x}^{\text{ad}} \mid \mathbf{Z}),$$

and assume $\pi_{\mathbf{a}, \mathbf{x}^{\text{ad}}}(\mathbf{Z}) > 0$ almost surely.

Lemma B.1 (IPW identity with joint propensity score). *For any integrable function $H(\mathbf{A}, \mathbf{X}^{\text{ad}}, \mathbf{Z}, \mathbf{X}^{\text{re}})$,*

$$\mathbb{E} \left[\frac{\mathbf{I}(\mathbf{A} = \mathbf{a}, \mathbf{X}^{\text{ad}} = \mathbf{x}^{\text{ad}})}{\pi_{\mathbf{a}, \mathbf{x}^{\text{ad}}}(\mathbf{Z})} \mathbb{E}_{\mathbf{X}^{\text{re}} \mid \mathbf{A}, \mathbf{X}^{\text{ad}}, \mathbf{Z}} \left[H(\mathbf{A}, \mathbf{X}^{\text{ad}}, \mathbf{Z}, \mathbf{X}^{\text{re}}) \right] \right] = \mathbb{E}_{\mathbf{Z}} \left[\mathbb{E}_{\mathbf{X}^{\text{re}} \mid \mathbf{A} = \mathbf{a}, \mathbf{X}^{\text{ad}} = \mathbf{x}^{\text{ad}}, \mathbf{Z}} \left[H(\mathbf{a}, \mathbf{x}^{\text{ad}}, \mathbf{Z}, \mathbf{X}^{\text{re}}) \right] \right]. \quad (15)$$

Proof. By the law of iterated expectations,

$$\begin{aligned} \mathbb{E} \left[\frac{\mathbf{I}(\mathbf{A} = \mathbf{a}, \mathbf{X}^{\text{ad}} = \mathbf{x}^{\text{ad}})}{\pi_{\mathbf{a}, \mathbf{x}^{\text{ad}}}(\mathbf{Z})} \mathbb{E}_{\mathbf{X}^{\text{re}} \mid \mathbf{A}, \mathbf{X}^{\text{ad}}, \mathbf{Z}} [H] \right] &= \mathbb{E}_{\mathbf{Z}} \left[\mathbb{E} \left[\frac{\mathbf{I}(\mathbf{A} = \mathbf{a}, \mathbf{X}^{\text{ad}} = \mathbf{x}^{\text{ad}})}{\pi_{\mathbf{a}, \mathbf{x}^{\text{ad}}}(\mathbf{Z})} \mathbb{E}_{\mathbf{X}^{\text{re}} \mid \mathbf{A}, \mathbf{X}^{\text{ad}}, \mathbf{Z}} [H] \mid \mathbf{Z} \right] \right] \\ &= \mathbb{E}_{\mathbf{Z}} \left[\frac{1}{\pi_{\mathbf{a}, \mathbf{x}^{\text{ad}}}(\mathbf{Z})} \mathbb{E} \left[\mathbf{I}(\mathbf{A} = \mathbf{a}, \mathbf{X}^{\text{ad}} = \mathbf{x}^{\text{ad}}) \mathbb{E}_{\mathbf{X}^{\text{re}} \mid \mathbf{A}, \mathbf{X}^{\text{ad}}, \mathbf{Z}} [H] \mid \mathbf{Z} \right] \right]. \end{aligned}$$

Conditioned on \mathbf{Z} , the indicator selects the event $(\mathbf{A}, \mathbf{X}^{\text{ad}}) = (\mathbf{a}, \mathbf{x}^{\text{ad}})$, hence

$$\mathbb{E} \left[\mathbf{I}(\mathbf{A} = \mathbf{a}, \mathbf{X}^{\text{ad}} = \mathbf{x}^{\text{ad}}) \mathbb{E}_{\mathbf{X}^{\text{re}} \mid \mathbf{A}, \mathbf{X}^{\text{ad}}, \mathbf{Z}} [H] \mid \mathbf{Z} \right] = P(\mathbf{A} = \mathbf{a}, \mathbf{X}^{\text{ad}} = \mathbf{x}^{\text{ad}} \mid \mathbf{Z}) \mathbb{E}_{\mathbf{X}^{\text{re}} \mid \mathbf{A} = \mathbf{a}, \mathbf{X}^{\text{ad}} = \mathbf{x}^{\text{ad}}, \mathbf{Z}} [H(\mathbf{a}, \mathbf{x}^{\text{ad}}, \mathbf{Z}, \mathbf{X}^{\text{re}})].$$

Since $P(\mathbf{A} = \mathbf{a}, \mathbf{X}^{\text{ad}} = \mathbf{x}^{\text{ad}} \mid \mathbf{Z}) = \pi_{\mathbf{a}, \mathbf{x}^{\text{ad}}}(\mathbf{Z})$, the factor cancels out, yielding (15). \square

By applying Lemma B.1 to $H(\mathbf{A}, \mathbf{X}^{\text{ad}}, \mathbf{Z}, \mathbf{X}^{\text{re}}) = P(\hat{Y} = \hat{y} \mid \mathbf{A}, \mathbf{X}^{\text{ad}}, \mathbf{Z}, \mathbf{X}^{\text{re}})$, the right-hand side of (14) is rewritten as

$$\mathbb{E} \left[\frac{\mathbf{I}(\mathbf{A} = \mathbf{a}, \mathbf{X}^{\text{ad}} = \mathbf{x}^{\text{ad}})}{\pi_{\mathbf{a}, \mathbf{x}^{\text{ad}}}(\mathbf{Z})} \mathbb{E}_{\mathbf{X}^{\text{re}} \mid \mathbf{A}, \mathbf{X}^{\text{ad}}, \mathbf{Z}} \left[P(\hat{Y} = \hat{y} \mid \mathbf{A}, \mathbf{X}^{\text{ad}}, \mathbf{Z}, \mathbf{X}^{\text{re}}) \right] \right], \quad (16)$$

which is Eq. (10).

C PROOF OF THEOREM 3.5

C.1 LEMMAS

We first present two lemmas that will be used in the proof of Theorem 3.5.

Lemma C.1 (Marg forbids an unshielded collider). *Assume $\mathbf{U}-\mathbf{A}-\mathbf{V}$ is an unshielded triple (i.e., \mathbf{U} and \mathbf{V} are non-adjacent) and $\mathcal{A}_{\langle \mathbf{U}, \mathbf{A}, \mathbf{V} \rangle} = \text{marg}$. Then no cluster DAG consistent with \mathcal{G} can contain the collider $\mathbf{U} \rightarrow \mathbf{A} \leftarrow \mathbf{V}$.*

Proof. From Anand et al. [2025, Remark 1], marginally-connecting independence arc marg always implies a non-collider structure. Hence, the triplet $\mathbf{U} - \mathbf{A} - \mathbf{V}$ must form a non-collider structure at the middle node \mathbf{A} , and the collider structure $\mathbf{U} \rightarrow \mathbf{A} \leftarrow \mathbf{V}$ is impossible. \square

Lemma C.2 (A back-path forces a directed cycle). *Let G be any cluster DAG that contains G_{\rightarrow} as a subgraph. If $\mathbf{U} \rightarrow \mathbf{A}$ and $\mathbf{A} \rightarrow \mathbf{V}$ are edges in G and there exists a directed path $\mathbf{V} \rightarrow \cdots \rightarrow \mathbf{U}$ in G_{\rightarrow} , then G contains a directed cycle.*

Proof. All directed edges in G_{\rightarrow} appear in G , hence the path $\mathbf{V} \rightarrow \cdots \rightarrow \mathbf{U}$ exists in G . Together with $\mathbf{A} \rightarrow \mathbf{V}$ and $\mathbf{U} \rightarrow \mathbf{A}$, we obtain the directed cycle $\mathbf{A} \rightarrow \mathbf{V} \rightarrow \cdots \rightarrow \mathbf{U} \rightarrow \mathbf{A}$. \square

C.2 PROOF

We restate Theorem 3.5 below for completeness and provide its proof.

Theorem C.3: *A set of clusters $S \subseteq \text{sib}(\mathbf{A}, \mathcal{G}) := \{\mathbf{C} \in \mathcal{C} : \mathbf{C} - \mathbf{A} \text{ in } \mathcal{G}\}$ in a cluster CPDAG \mathcal{G} is a possible parent set of \mathbf{A} if and only if it satisfies the following two conditions:*

1. **Collider-structure compatibility:** *All distinct $\mathbf{U}, \mathbf{V} \in S$ satisfy either (i) \mathbf{U} and \mathbf{V} are adjacent, or (ii) \mathbf{U} and \mathbf{V} are not adjacent and $\mathcal{A}_{\langle \mathbf{U}, \mathbf{A}, \mathbf{V} \rangle} = \text{never}$.*
2. **No back-path condition:** *Let $\mathcal{G}_{\rightarrow}$ be the directed subgraph of \mathcal{G} obtained by removing all undirected edges. For every $\mathbf{U} \in S$ and every $\mathbf{V} \in \text{sib}(\mathbf{A}, \mathcal{G}) \setminus S$, there is no directed path from \mathbf{V} to \mathbf{U} in $\mathcal{G}_{\rightarrow}$.*

Proof of Theorem. (\Rightarrow) Assume that S is a possible parent set of \mathbf{A} . Then there exists a cluster DAG G in the cluster MEC represented by \mathcal{G} such that $\mathbf{U} \rightarrow \mathbf{A}$ for all $\mathbf{U} \in S$ and $\mathbf{A} \rightarrow \mathbf{V}$ for all $\mathbf{V} \in \text{sib}(\mathbf{A}, \mathcal{G}) \setminus S$.

(1) Take distinct $\mathbf{U}, \mathbf{V} \in S$. If they are adjacent, we are done. If they are non-adjacent, then $\mathbf{U} \rightarrow \mathbf{A} \leftarrow \mathbf{V}$ is an unshielded collider in G . By Lemma C.1, we cannot have $\mathcal{A}_{\langle \mathbf{U}, \mathbf{A}, \mathbf{V} \rangle} = \text{marg}$. Moreover, $\mathcal{A}_{\langle \mathbf{U}, \mathbf{A}, \mathbf{V} \rangle} = \text{cond}$ would compel the collider in every DAG in the MEC, implying both edges into \mathbf{A} are directed in \mathcal{G} , contradicting that \mathbf{U}, \mathbf{V} are siblings (connected to \mathbf{A} by undirected edges). Hence $\mathcal{A}_{\langle \mathbf{U}, \mathbf{A}, \mathbf{V} \rangle} = \text{never}$.

(2) Take $\mathbf{U} \in S$ and $\mathbf{V} \in \text{sib}(\mathbf{A}, \mathcal{G}) \setminus S$. If there were a directed path $\mathbf{V} \rightarrow \cdots \rightarrow \mathbf{U}$ in $\mathcal{G}_{\rightarrow}$, then Lemma C.2 would yield a directed cycle in G , contradicting acyclicity. Thus no such path exists.

(\Leftarrow) Assume Conditions (1)–(2). Orient each undirected edge incident to \mathbf{A} as $\mathbf{U} \rightarrow \mathbf{A}$ for $\mathbf{U} \in S$ and $\mathbf{A} \rightarrow \mathbf{V}$ for $\mathbf{V} \in \text{sib}(\mathbf{A}, \mathcal{G}) \setminus S$. Condition (1) ensures that any unshielded collider created at \mathbf{A} is allowed (i.e., it occurs only when the corresponding independence arc is never), so no independence-arc constraint at \mathbf{A} is violated. Condition (2) rules out a back-path in $\mathcal{G}_{\rightarrow}$ that would force a directed cycle once we impose $\mathbf{U} \rightarrow \mathbf{A}$ and $\mathbf{A} \rightarrow \mathbf{V}$; see Lemma C.2.

Since \mathcal{G} represents a nonempty cluster MEC and our imposed orientations do not contradict the fixed constraints (i.e., independence-arc constraints and acyclicity constraints), there exists at least one cluster DAG extension G in the MEC realizing these orientations. In that G , the parents of \mathbf{A} among its siblings are exactly S . Hence S is a possible parent set of \mathbf{A} . \square

D EXPERIMENTAL SETTINGS

D.1 BASELINES

In our experiments, we compare the performance of our method (**C-IFair**) with six baselines:

- **Full**, which trains the prediction model with the full feature set without any fairness constraint.
- **Unaware**, which trains the prediction model using all features except the sensitive features A .
- **No-DesCs**, which trains the prediction model using all features except definite descendant clusters of sensitive features A . To choose such clusters, we first apply the CLOC algorithm [Anand et al., 2025] to learn the cluster CPDAG from data, and then identify the definite descendant clusters of A as the clusters that can be reached from A via directed paths.
- **ϵ -IFair** [Zuo et al., 2024], which aims to reduce the kernel MMD between the interventional distributions that are estimated based on the decomposition formula given by the partial causal ordering (PCO) algorithm [Perkovic, 2020]. We employ the publicly available implementation downloaded from <https://github.com/aoqiz/Interventional-Fairness-with-Partially-Known-Causal-Graphs>.
- **ℓ -IFair** [Li et al., 2024], which estimates a conditional average treatment effect (CATE) of A on prediction \hat{Y} for all observed values of features X and then penalizes their maximum to ensure interventional fairness. These CATE estimates are given by multiple adjustment sets, each obtained by the local search over a CPDAG. We use the source codes on <https://github.com/haoxuanli-pku/NeurIPS24-Interventional-Fairness-with-PDAGs>.
- **Oracle**, which trains the prediction model using all features except the non-descendant variables of sensitive features A . This method serves as an oracle baseline, as it chooses such input features based on the true variable-level causal graph, which is unavailable in practice.

D.2 SETTINGS OF EACH METHOD

- **Model choice:** As the prediction model for each method, we use a two-layer multi-layer perceptron (MLP) with rectified linear unit (ReLU) activation and 32 hidden units for all datasets. For our **C-IFair** method, we parameterize the propensity score model $\pi_{a, x^{\text{ad}}}(\mathbf{Z}) := P(A = a, X^{\text{ad}} = x^{\text{ad}} | \mathbf{Z})$ using a two-layer MLP with ReLU activation and 64 hidden units. In all experiments, we obtain IPW weights by applying self-normalization, which divides each IPW weight by its empirical average; in Section E.6, we present sensitivity analyses of our method to weight clipping.
- **Hyperparameters:**
 - **Training settings for prediction models:** For all methods, we set the batch size to 256, the number of training epochs to 1000, the learning rate to $\text{lr} = 10^{-3}$.
 - **Optimization algorithm:** For our **C-IFair** method, we can use any gradient-based stochastic optimization algorithm. In our experiments, we use the AdamW algorithm [Loshchilov and Hutter, 2019] in PyTorch.
 - **Kernel choice:** For our **C-IFair** method, we use the Gaussian kernel with multiple bandwidths $c_\gamma \gamma$, where $c_\gamma \in [0.5, 1.0, 2.0, 4.0, 8.0, 16.0]$, and γ is selected using the standard heuristic called the *median heuristic* [Gretton et al., 2012]. We set the number of RFFs to $d_{\text{RFF}} = 128$.
 - **Unfairness penalty:** For our **C-IFair**, we select the unfairness penalty parameter λ from $\{0., 2.0, \dots, 20.0\}$ based on the validation set. In the accuracy-fairness trade-off curve (Figure 3), we vary λ in $[0, 1, 2, 5, 10, 20, 50, 100, 200]$. We fix the temperature parameter ω in the Mellowmax function [Asadi and Littman, 2017] to $\omega = 10.0$ for all experiments. For **ϵ -IFair** and **ℓ -IFair**, we choose their penalty parameter values from the suggested value ranges in Zuo et al. [2024] and Li et al. [2024] to achieve their best performance.
- **CPDAG inference:** To infer a cluster CPDAG for our **C-IFair** method, we apply the CLOC algorithm [Anand et al., 2025] by employing the Fisher-z’s test in the Python package `causal-learn` [Zheng et al., 2024] with significance level $\alpha = 0.01$. To learn a variable-level CPDAG for **ℓ -IFair**, we run the Peter-Clark (PC) algorithm [Spirtes et al., 2000] implemented in `causal-learn` [Zheng et al., 2024] using the Fisher-z’ test with $\alpha = 0.01$. Regarding **ϵ -IFair**, following the official implementation with default settings, we run the greedy equivalence search (GES) algorithm [Chickering, 2002] implemented in a general causal discovery software named TETRAD [Ramsey et al., 2018].

D.3 SYNTHETIC DATA GENERATION PROCESSES

This section describes the generation processes of the synthetic datasets used in Section 4.1.

D.3.1 Causal Graph Generation and Cluster Partition

We randomly generate the ground truth variable-level causal DAGs G_v by sampling the ER model with expected node degree 2.

To obtain a cluster DAG G , we follow its definition (Section 2.3): we draw an edge $C_i \rightarrow C_j$ in the cluster DAG G if there exists at least one edge $V_i \rightarrow V_j$ in the variable-level DAG G_v such that $V_i \in C_i$ and $V_j \in C_j$. To construct a partition of clusters $\mathcal{C} = \{C_1, \dots, C_d\}$, we randomly assign 3 variable nodes in G_v to one of the clusters.

We randomly choose the sensitive cluster A from the clusters with degree more than or equal to 2. In our experiments with admissible features (Section E.1), we randomly choose admissible features X^{ad} from the children of sensitive features A in the cluster DAG G .

We treat A and X^{ad} as binary clusters and Y as a continuous cluster. For the remaining clusters, we randomly choose binary and continuous clusters.

D.3.2 Linear Datasets

Using the random causal graphs described in Section D.3.1, we generate linear datasets as follows.

To generate the values of features X , we sample them using a linear SCM associated with the variable-level DAG G_v . For each continuous variable X_v , we sample its value from the following linear structural equation:

$$X_v = \sum_{u \in \text{pa}(v)} w_{v,u} X_u + \varepsilon_v,$$

where the noise is sampled from the standard Gaussian distribution $\varepsilon_v \sim \mathcal{N}(0, 1)$, and each linear coefficient $w_{v,u}$ are given by $w_{v,u} = s_{v,u} m_{v,u}$, where

$$s_{v,u} \sim \text{Unif}\{-1, +1\}, \quad m_{v,u} \sim \text{Unif}(0.5, 2.0).$$

For each binary variable X_v , we sample its value from the following structural equation:

$$X_v \sim \text{Bernoulli} \left(\sigma \left(\sum_{u \in \text{pa}(v)} w_{v,u} X_u \right) \right), \quad \sigma(t) = \frac{1}{1 + e^{-t}}.$$

To generate the values of target variable Y , we use the following linear structural equation:

$$Y_v = \sum_{u \in \text{pa}(v)} w_{v,u} X_u + \varepsilon_v,$$

where the noise is sampled from the standard Gaussian distribution $\varepsilon_v \sim \mathcal{N}(0, 1)$, the parent set $\text{pa}(v)$ is forced to include all feature clusters, and each linear coefficient $w_{v,u}$ is given by $w_{v,u} = s_{v,u} m_{v,u}$ when u is not sensitive cluster A ; otherwise, we set $w_{v,u} = 5s_{v,u} m_{v,u}$ to introduce unfair bias.

D.3.3 Nonlinear Datasets

We generate nonlinear datasets in the same way as linear dataset generation processes described in Section D.3.2, except that we apply nonlinear function $\xi(\cdot)$ for all variables that have parents in the variable-level DAG G_v .

Instead of the linear function $\sum_{u \in \text{pa}(v)} w_{v,u} X_u$, we use the following nonlinear function:

$$\xi \left(\sum_{u \in \text{pa}(v)} w_{v,u} X_u \right),$$

where nonlinear function $\xi(t)$ is randomly chosen from $\xi(t) = \sin(t)$, $\xi(t) = \cos(t)$, and $\xi(t) = \tanh(t)$.

D.4 REAL-WORLD DATA

We use the Adult, German credit, and Open University Learning Analytics Dataset (OULAD) dataset downloaded from the University of California, Irvine (UCI) repository [Bache and Lichman, 2013].

Adult Dataset. The Adult dataset contains 48,842 instances with 14 attributes, where the task is to predict whether an individual’s income exceeds \$50,000 per year. We treat gender A_1 and race A_2 as sensitive features $\mathbf{A} = [A_1, A_2]$, where $A_1 = 0$ and $A_1 = 1$ represent female and male, respectively, and $A_2 = 0$ and $A_2 = 1$ represent not White (i.e., all other race categories grouped) and White, respectively. We manually construct a cluster partition based on the domain knowledge of the Adult dataset. Specifically, we group related features into clusters by grouping the attributes of family background (i.e., marital-status and relationship) as one cluster, and the attributes of demographic information (i.e., education and native-country) as another cluster. Other features are treated as singleton-node clusters.

German Credit Dataset. The German credit dataset contains 1,000 instances with 20 attributes, where the task is to classify people described by a set of attributes as good or bad credit risks. We treat gender and age as sensitive features \mathbf{A} . We group the attributes of financial information (i.e., credit amount and duration) as one cluster. Other features are treated as singleton-node clusters.

OULAD Dataset. The OULAD dataset contains the records about 32,593 students with 7 attributes, where the task is to predict whether a student will pass a course. We treat disability as sensitive feature \mathbf{A} . Here we treat all features as singleton-node clusters, as the OULAD dataset contains only a small number of features.

Causal Graphs. Since the ground-truth causal graph structures are **unknown** for these real-world datasets, we use the causal graphs provided by previous works that have been constructed based on domain knowledge or data-driven causal discovery methods. For the Adult, German credit, and OULAD datasets, we use the causal graphs provided by Zhang et al. [2017], Watson et al. [2021], and Kim and Kim [2025], respectively. Based on these causal graphs, we identify the back-door adjustment sets to use the IPW-based estimator for the kernel MMD evaluation.

D.5 PERFORMANCE METRICS

To evaluate the performance of each method, we use the following metrics:

- Root mean squared error (**RMSE**), which measures the error between predicted and true target values.
- Area under the (receiver operating characteristic) curve (**AUC**), which measures the classification performance. By focusing on the ranking of predictions rather than absolute accuracy, it remains robust even with imbalanced datasets.
- **Unfairness**, which measures the interventional unfairness based on the kernel MMD between interventional distributions of prediction \hat{Y} under different sensitive feature values. In our synthetic data experiments, we estimate the empirical kernel MMDs by sampling the values of input features X under interventions from the true interventional distributions obtained with the ground-truth SCM parameters. In real-world data experiments, we estimate the kernel MMDs using IPW (Section 3.3.2) with valid adjustment set Z identified from the provided causal graph structures (Section D.4).

D.6 COMPUTING INFRASTRUCTURE

In our runtime computation experiments (Section E.5), we used a 64-bit Ubuntu machine with 2.30GHz Xeon Gold 5218 32-core (x2) CPUs, NVIDIA TITAN RTX (x4) GPUs, and 256-GB RAM.

E ADDITIONAL EXPERIMENTS

This section presents additional experimental results for further validating the effectiveness of our **C-IFair** method.

E.1 EXPERIMENTS WITH ADMISSIBLE FEATURES

Admissible features are the features through which the effect of sensitive features \mathbf{A} is **not** treated as unfair, due to the requirement of the application domain (see the motivating example scenario illustrated in Section 2.2). Although the use of

Table 3: RMSE and unfairness for linear (top) and nonlinear (bottom) datasets with admissible features on held-out test set.

LINEAR	$d=5 (d_v=15)$		$d=10 (d_v=30)$		$d=15 (d_v=45)$	
	RMSE↓	UNFAIRNESS↓	RMSE↓	UNFAIRNESS↓	RMSE↓	UNFAIRNESS↓
ORACLE	0.985 ± 0.056	0.000 ± 0.000	0.795 ± 0.090	0.000 ± 0.000	0.879 ± 0.093	0.000 ± 0.000
FULL	0.559 ± 0.090	0.244 ± 0.112	0.553 ± 0.148	0.065 ± 0.022	0.657 ± 0.430	0.071 ± 0.054
UNAWARE	0.805 ± 0.104	0.083 ± 0.062	0.773 ± 0.211	0.035 ± 0.020	0.917 ± 0.141	0.034 ± 0.023
NO-DESCs	0.797 ± 0.112	0.085 ± 0.065	0.591 ± 0.105	0.038 ± 0.008	0.759 ± 0.191	0.064 ± 0.056
ϵ -IFAIR	0.786 ± 0.043	0.099 ± 0.082	0.600 ± 0.064	0.026 ± 0.011	0.750 ± 0.103	0.039 ± 0.003
C-IFAIR	0.777 ± 0.061	0.058 ± 0.060	0.581 ± 0.087	0.015 ± 0.009	0.728 ± 0.076	0.024 ± 0.026

NONLINEAR	$d=5 (d_v=15)$		$d=10 (d_v=30)$		$d=15 (d_v=45)$	
	RMSE↓	UNFAIRNESS↓	RMSE↓	UNFAIRNESS↓	RMSE↓	UNFAIRNESS↓
ORACLE	1.099 ± 0.056	0.000 ± 0.000	1.083 ± 0.086	0.000 ± 0.000	1.071 ± 0.105	0.000 ± 0.000
FULL	0.953 ± 0.144	0.089 ± 0.062	0.973 ± 0.124	0.062 ± 0.010	0.989 ± 0.226	0.055 ± 0.006
UNAWARE	0.994 ± 0.064	0.074 ± 0.057	0.959 ± 0.086	0.032 ± 0.010	1.065 ± 0.129	0.025 ± 0.010
NO-DESCs	0.991 ± 0.063	0.061 ± 0.047	0.948 ± 0.085	0.023 ± 0.011	1.071 ± 0.170	0.027 ± 0.017
ϵ -IFAIR	0.996 ± 0.070	0.097 ± 0.019	0.960 ± 0.078	0.025 ± 0.004	1.019 ± 0.046	0.021 ± 0.009
C-IFAIR	0.989 ± 0.062	0.046 ± 0.081	0.947 ± 0.104	0.021 ± 0.002	1.003 ± 0.075	0.019 ± 0.007

admissible features can be beneficial for improving the prediction performance, it becomes more challenging to achieve interventional fairness, as the presence of admissible features increases the number of interventional distribution pairs.

Below we evaluate the performance of **C-IFair** method in the presence of such admissible features.

Data. We use linear and nonlinear synthetic datasets generated in the same way as described in Section D.3, except that we randomly choose admissible feature cluster X^{ad} of 3 binary variables from the children of sensitive features A in the cluster DAG G .

Baselines. In this experiment, we do not compare **C-IFair** method with ℓ -**IFair**, as its publicly available implementation does not support the setting with admissible features. For the remaining five baselines presented in Section D.1, we use the same settings as described in Section D.2.

Results. Table 3 presents the mean and standard deviation of RMSE and unfairness over 20 synthetic datasets with admissible features.

Despite the increase in the number of interventional distribution pairs, our **C-IFair** again achieves the best performance in terms of both RMSE and unfairness across all settings, underscoring the effectiveness of our unfairness penalty formulation. Notably, compared with ϵ -**IFair**, which aims to reduce the kernel MMD estimated by approximately sampling interventional datasets for each value pair of intervened variables A and X^{ad} , our **C-IFair** method consistently yields fairer predictions (particularly on linear datasets), highlighting the advantage of our barycenter kernel MMD formulation in handling the increased number of interventional distribution pairs.

E.2 EXPERIMENTS UNDER DENSE CLUSTER GRAPHS

To measure unfairness, our **C-IFair** method infers interventional distributions using adjustment cluster sets identified from the cluster CPDAG (Section 3.2). Since these sets rely on the number of possible parent sets for sensitive features A (i.e., S^1, \dots, S^M), their number M increases when the number of undirected edges incident to A grows, which can make it more difficult to achieve interventional fairness.

To test our **C-IFair** under such cases, we conduct experiments using synthetic datasets generated from dense graphs.

Data. We use synthetic datasets generated in the same way as described in Section D.3, except that we generate the underlying variable-level DAGs G_v using the ER model with expected node degree $p = 4$ to make the cluster graphs denser. We set the number of clusters to $d = 10, 15$, as setting $d = 5$ substantially reduces the randomness of the ER model.

Table 4: RMSE and unfairness on synthetic datasets generated using dense causal graphs

LINEAR	$d=10$		$d=15$	
	RMSE↓	UNFAIRNESS↓	RMSE↓	UNFAIRNESS↓
ORACLE	0.707 ± 0.147	0.000 ± 0.000	0.727 ± 0.173	0.000 ± 0.000
FULL	0.470 ± 0.127	0.099 ± 0.079	0.492 ± 0.113	0.061 ± 0.045
UNAWARE	0.730 ± 0.222	0.048 ± 0.029	0.928 ± 0.066	0.023 ± 0.049
NO-DESCS	0.571 ± 0.114	0.047 ± 0.055	0.504 ± 0.096	0.026 ± 0.013
ϵ -IFAIR	0.689 ± 0.099	0.124 ± 0.060	0.503 ± 0.073	0.302 ± 0.109
ℓ -IFAIR	0.669 ± 0.295	0.077 ± 0.053	0.767 ± 0.241	0.044 ± 0.033
C-IFAIR	0.550 ± 0.074	0.040 ± 0.061	0.498 ± 0.121	0.020 ± 0.011

NONLINEAR	$d=10$		$d=15$	
	RMSE↓	UNFAIRNESS↓	RMSE↓	UNFAIRNESS↓
ORACLE	0.976 ± 0.045	0.000 ± 0.000	0.978 ± 0.041	0.000 ± 0.000
FULL	0.807 ± 0.051	0.022 ± 0.010	0.870 ± 0.054	0.019 ± 0.006
UNAWARE	0.988 ± 0.059	0.021 ± 0.024	0.996 ± 0.031	0.005 ± 0.005
NO-DESCS	0.990 ± 0.052	0.016 ± 0.015	0.985 ± 0.057	0.006 ± 0.002
ϵ -IFAIR	0.999 ± 0.019	0.024 ± 0.005	0.916 ± 0.051	0.077 ± 0.046
ℓ -IFAIR	0.989 ± 0.056	0.014 ± 0.001	1.082 ± 0.002	0.006 ± 0.000
C-IFAIR	0.985 ± 0.027	0.011 ± 0.002	0.976 ± 0.023	0.005 ± 0.002

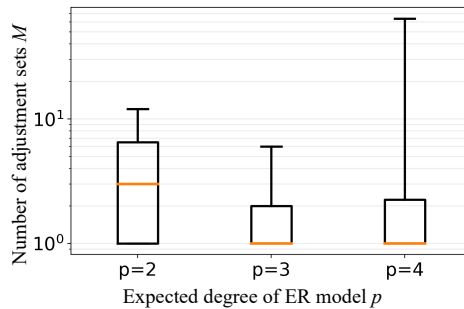


Figure 5: Log-scale box plot of number of adjustment sets M for expected node degree p on linear datasets with $d = 10$ clusters. Whiskers, boxes, and orange lines denote minimum and maximum, interquartile range, and median, respectively.

Graph Density and Number of Adjustment Sets. Before making performance comparisons, we analyze the relationship between the density of cluster graphs and the number of adjustment sets M .

Figure 5 presents the log-scale box plot of the number of adjustment sets M for expected node degree $p = 2, 3,$ and 4 in the ER model on the linear synthetic datasets with $d = 10$ clusters.

Surprisingly, on average, the number of adjustment sets M decreases as the expected node degree p increases. This is mainly because the number of adjustment sets M is determined not necessarily by the overall graph density, but rather by the number of **undirected** edges incident to sensitive features A .

In particular, when we perform graph refinement (Section 3.2.3), the number of undirected edges in the cluster CPDAG can sharply decrease, implying that cluster refinement can also help disambiguate the causal relationships around sensitive features A and thus reduce the number of adjustment sets M . This observation is consistent with the example of variable-level and cluster CPDAGs in Figure 1 (c) and (e), where the cluster CPDAG has 2 undirected edges incident to A , whereas the variable-level CPDAG has only 1 undirected edge incident to A , despite the increase in the graph size.

However, on some datasets with $p = 4$, graph refinement does not occur, and the number of adjustment sets M can be as large as $M = 64$. Below we compare the performance of each method under $p = 4$.

Results. Table 4 presents the mean and standard deviation of RMSE and unfairness over 20 synthetic datasets.

Table 5: RMSE and unfairness on linear synthetic datasets: For our **C-IFair** (and **No-DesCs**), we use a cluster CPDAG inferred with an inadmissible partition. Since no method achieves **both** lowest RMSE and unfairness, we do not bold any result in this table.

METHOD	$d=5$		$d=10$		$d=15$	
	RMSE↓	UNFAIRNESS↓	RMSE↓	UNFAIRNESS↓	RMSE↓	UNFAIRNESS↓
ORACLE	0.949 ± 0.096	0.000 ± 0.000	0.758 ± 0.115	0.000 ± 0.000	0.702 ± 0.123	0.000 ± 0.000
FULL	0.484 ± 0.203	0.239 ± 0.218	0.522 ± 0.174	0.100 ± 0.073	0.617 ± 0.207	0.073 ± 0.062
UNAWARE	0.709 ± 0.191	0.071 ± 0.061	0.753 ± 0.156	0.034 ± 0.051	0.782 ± 0.121	0.035 ± 0.070
NO-DESCS	0.694 ± 0.188	0.069 ± 0.050	0.615 ± 0.135	0.042 ± 0.039	0.631 ± 0.142	0.031 ± 0.028
ϵ -IFAIR	0.718 ± 0.124	0.172 ± 0.004	0.654 ± 0.152	0.097 ± 0.015	0.561 ± 0.093	0.091 ± 0.016
ℓ -IFAIR	0.719 ± 0.332	0.064 ± 0.006	0.703 ± 0.004	0.127 ± 0.104	0.624 ± 0.030	0.086 ± 0.027
C-IFAIR	0.705 ± 0.189	0.072 ± 0.072	0.622 ± 0.117	0.041 ± 0.038	0.637 ± 0.177	0.027 ± 0.028

Our **C-IFair** method again achieves the best performance in terms of both RMSE and unfairness across all settings, demonstrating its effectiveness even under dense cluster graphs. Although ℓ -**IFair** also performs parent-set-based adjustment using a variable-level CPDAG, it produces unfairer predictions than our **C-IFair** method, particularly on linear datasets, which may be attributed to the fact that the variable-level CPDAGs inferred by the PC algorithm are less accurate than the cluster CPDAGs inferred by the CLOC algorithm, as we will describe in Section E.5.

Notably, ϵ -**IFair** yields the worst performance in terms of unfairness in all settings, due to the significant violation of its assumption for adjustment, which requires that no features in X are connected to sensitive features A via undirected edges in the variable-level CPDAG. By contrast, our **C-IFair** method does not require such a demanding assumption, and thus can strike the best balance between prediction accuracy and fairness, even under dense cluster graphs.

E.3 EMPIRICAL ROBUSTNESS TO ASSUMPTION VIOLATION

Our **C-IFair** method relies on the cluster CPDAG inferred by the CLOC algorithm [Anand et al., 2025], which requires the three assumptions described in Section 3.2.1. Compared with the assumptions required by ϵ -**IFair** and ℓ -**IFair**, Assumption 3.2 is an additional assumption that is not needed by these methods.

This assumption requires that the cluster partition used for inferring the cluster CPDAG is admissible, which means that partitioning the nodes in the variable-level causal DAG does not yield any directed cycle in the cluster graph. Since the partition is given by a user in practical applications, this assumption can be violated when the domain knowledge of the relationships among features is limited. Theoretically, CLOC cannot guarantee the identifiability of the cluster CPDAG in such cases, and thus the validity of the adjustment sets identified from the cluster CPDAG is not guaranteed.

Below we empirically evaluate the robustness of our **C-IFair** to the violation of Assumption 3.2, using linear synthetic datasets.

Data and Causal Graphs. We generate linear synthetic datasets in the same way as described in Section D.3. Based on the underlying variable-level DAGs G_v generated from the ER model with expected node degree 2, we force the cluster partition to be *inadmissible* by taking two steps:

- We seek two node pairs (U_i, V_i) and (U_j, V_j) from the variable-level DAG G_v such that $U_i \rightarrow U_j$ and $V_i \leftarrow V_j$.
- Then we force the cluster partition to assign (U_i, V_i) to one cluster C_i and (U_j, V_j) to another cluster C_j , which yields a directed cycle (i.e., $C_i \rightarrow C_j$ and $C_i \leftarrow C_j$) in the ground-truth cluster graph.

Using such partition $\mathcal{C} = \{C_1, \dots, C_d\}$, we infer a cluster CPDAG using the CLOC algorithm, and then apply our **C-IFair** method (and **No-DesCs**) using the inferred cluster CPDAG.

To focus on the violation of Assumption 3.2, we do **not** use nonlinear synthetic datasets, as the complex nonlinearity affects the accuracy of conditional independence tests used for inferring the cluster CPDAG, which can make it difficult to isolate the effect of the violation of Assumption 3.2 on the performance of our **C-IFair** method.

Results. Table 5 presents the mean and standard deviation of RMSE and unfairness over 20 linear synthetic datasets.

Table 6: RMSE and unfairness on held-out test set in linear synthetic datasets generated using causal DAG in Figure 6 (a).

	RMSE↓	UNFAIRNESS↓
ORACLE	0.756 ± 0.053	0.000 ± 0.000
FULL	0.256 ± 0.051	0.093 ± 0.083
UNAWARE	0.707 ± 0.158	0.054 ± 0.001
NO-DESCS	0.708 ± 0.158	0.044 ± 0.001
ϵ -IFAIR	0.435 ± 0.132	0.026 ± 0.004
ℓ -IFAIR	0.753 ± 0.224	0.027 ± 0.019
C-IFAIR	0.320 ± 0.115	0.025 ± 0.013

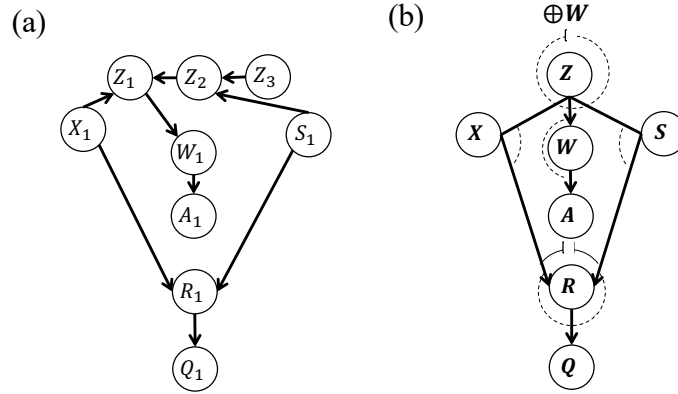


Figure 6: Specially designed causal graphs where parent of sensitive features A is annotated in connection mark: (a) variable-level ground-truth DAG over X , (b) cluster CPDAG over X with independence arcs and connection marks.

As expected, the performance of our **C-IFair** method decreases compared with the results in Table 1 (top), due to the inaccurate cluster CPDAG inferred with the inadmissible partition. However, our **C-IFair** method still achieves highly comparable performance to the baselines, and even outperforms some of them in terms of RMSE and unfairness, demonstrating its empirical robustness to the violation of Assumption 3.2. This might be attributed to the fact that, even with the violation of Assumption 3.2, the cluster CPDAG inferred by CLOC can still capture some of the true causal relationships among clusters, which can help identify some valid adjustment sets for estimating interventional distributions.

E.4 EXPERIMENTS INVOLVING CONNECTION MARKS

As described in Section 3.2, our strategy for obtaining adjustment sets is two-fold. We first enumerate a parent set of sensitive features A . If this set contains the clusters annotated with connection marks, then we augment it with additional clusters.

To validate this second stage, we evaluate the performance on synthetic datasets generated using the causal DAG in Figure 6 (a), where the parent of A (i.e., W) appears in a connection mark in the corresponding cluster CPDAG (Figure 6 (b)).

Data and Causal Graphs. We generate linear synthetic datasets using the same data generation process described in Section D.3, except that we use the causal DAG in Figure 6 (a) as the ground-truth variable-level DAG G_v .

We choose this causal graph from Anand et al. [2025, Figure 4 (c)], as its corresponding cluster CPDAG contains a cluster with a connection mark. We illustrate the cluster CPDAG in Figure 6 (b), as well as the independence arcs and connection marks. As shown in Figure 6, the number of variables and clusters are $d_v = 9$ and $d = 7$, respectively.

Results. Table 6 presents the mean and standard deviation of RMSE and unfairness over 20 synthetic datasets.

Our **C-IFair** strikes the best balance between RMSE and unfairness across baselines, implying that our adjustment cluster addition algorithm (Algorithm 1) successfully works to identify the valid adjustment sets.

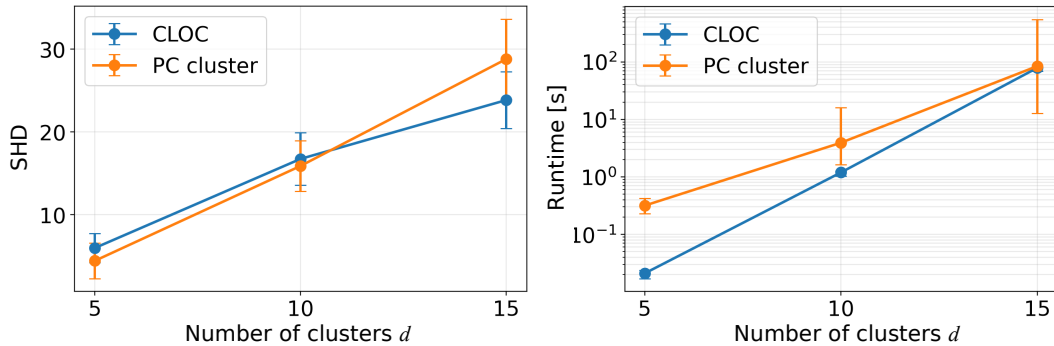


Figure 7: Performance comparison of CLOC with naive PC-based clustering on 20 linear synthetic datasets: (a) Mean and standard deviation of Structural Hamming distance (SHD) between the learned and true cluster DAGs; (b) Median and 25 / 75 percentiles of runtime [s] in a logarithmic scale.

E.5 GRAPH INFERENCE PERFORMANCE COMPARISON

To illustrate why our **C-IFair** yields better performance than the baseline based on the variable-level CPDAG (i.e., ℓ -**IFair**), we compare the performance of the CLOC algorithm with the PC algorithm in terms of both accuracy and runtime.

Baseline. We compare the CLOC algorithm with the *PC-then-cluster* approach in Anand et al. [2025], which first applies the PC algorithm to learn a variable-level CPDAG and then constructs a cluster CPDAG by grouping variables into clusters based on the pre-defined cluster partition.

Fairness and Objective of Performance Comparison. It is important to note that **we cannot make an entirely fair comparison** between the CLOC and PC algorithms, as their inference targets are **different**. As noted by Anand et al. [2025], the PC-then-cluster approach is **not** guaranteed to ensure that the learned cluster CPDAG belongs to the cluster MEC, even when all conditional independence tests are correct.

Moreover, we cannot easily jump to the conclusion that the CLOC’s better performance implies the better performance of our **C-IFair**, as the performance of ℓ -**IFair** does **not** depend on the performance of PC-then-cluster approach but on the performance of the PC algorithm itself.

Our objective here is to give an illustration of the potential performance gap between the CLOC and naive PC-then-cluster algorithms, which could be treated as indirect evidence for the better performance of our **C-IFair** than ℓ -**IFair**.

Results. Figure 7 presents the comparison of SHD and runtime between the CLOC and PC-then-cluster algorithms on 20 linear synthetic datasets.

As expected, the CLOC algorithm outperforms the PC-then-cluster approach in high-dimensional setups ($d = 15$), where our **C-IFair** also achieves better performance than ℓ -**IFair**. Notably, the runtime of the PC-then-cluster approach is substantially higher than that of the CLOC algorithm and highly variable across datasets particularly in high-dimensional setups ($d = 15$).

Such superior and stable performance justifies the use of the CLOC algorithm for cluster CPDAG inference in our **C-IFair**, which might be one of the key factors contributing to the better performance of our method than ℓ -**IFair**.

Discussion on time complexity. We conclude this section with a theoretical comparison of the worst-case time complexity of the CLOC and PC algorithms reported in the literature [Anand et al., 2025].

Anand et al. [2025] show that the worst-case time complexity of the CLOC algorithm is $O(d^2 2^p (d + p^2))$, where d is the number of clusters and p is the maximum of cluster degrees. By contrast, the standard PC algorithm requires the worst-case time complexity of $O(d_v^2 2^{p_v})$ where d_v is the number of variables, and p_v is the maximum degree of the variable-level DAG.

As discussed by Anand et al. [2025], these complexity results suggest that CLOC can be more efficient than PC when

1. the number of clusters d is much smaller than the number of variables d_v , and
2. inter-cluster connectivity is sparse (i.e., the maximum cluster degree p is not larger).

In real-world applications for algorithmic fairness, both of these conditions are often satisfied, as the number of clusters is typically much smaller than the number of variables, and inter-cluster connectivity is often sparse.

Hence, these theoretical insights imply that CLOC can be more efficient than the PC algorithm in practical applications. This efficiency justifies our refinement procedure for the cluster CPDAG using CLOC, described in Section 3.2.3.

E.6 SENSITIVITY ANALYSIS

Our **C-IFair** method measures the unfairness of predictions by employing the weighted kernel MMD estimators and taking their maximum over adjustment sets. This unfairness evaluation procedure involves two mechanisms: (i) the use of IPW weights for estimating interventional distributions, and (ii) the use of the Mellowmax function [Asadi and Littman, 2017] as a differentiable approximation of the maximum function.

To analyze the sensitivity to these two mechanisms, we evaluate the performance of our **C-IFair** method by varying the IPW clipping threshold and the Mellowmax temperature parameter ω .

Data. We use exactly the same linear synthetic datasets as described in Section D.3.

Evaluation Protocol. To evaluate the sensitivity to the IPW weights, we perform the clipping of (self-normalized) IPW weights. We clip the IPW weights using their q -th quantile in each mini-batch, where $q \in \{0.95, 0.975, 0.99\}$ and compare the performance with the case without clipping (i.e., $q = 1.0$).

To test the sensitivity to the Mellowmax function, we vary the temperature parameter ω of the Mellowmax function, which controls the smoothness of the approximation and approaches the maximum function as ω increases. We evaluate the performance with $\omega \in \{2.0, 10.0, 100.0\}$ and compare it with the variant of our method that does not use Mellowmax but takes the maximum over adjustment sets.

As described in Section D.2, in our main experiments, we do not perform IPW clipping and use the Mellowmax function with $\omega = 10.0$ as a default setting.

Results. Figures 8 and 9 present the average performance of our **C-IFair** method on 20 linear synthetic datasets when the IPW clipping threshold and the Mellowmax temperature parameter ω are varied.

We observe that the performance of our **C-IFair** method is not very sensitive to the IPW clipping or to the Mellowmax temperature value. However, our **C-IFair** method consistently achieves lower RMSE than the variant without Mellowmax (illustrated as the black dashed line in Figure 9), indicating that the use of Mellowmax function as differentiable approximation can help stabilize the gradient-based training and strike better balance between prediction accuracy and fairness.

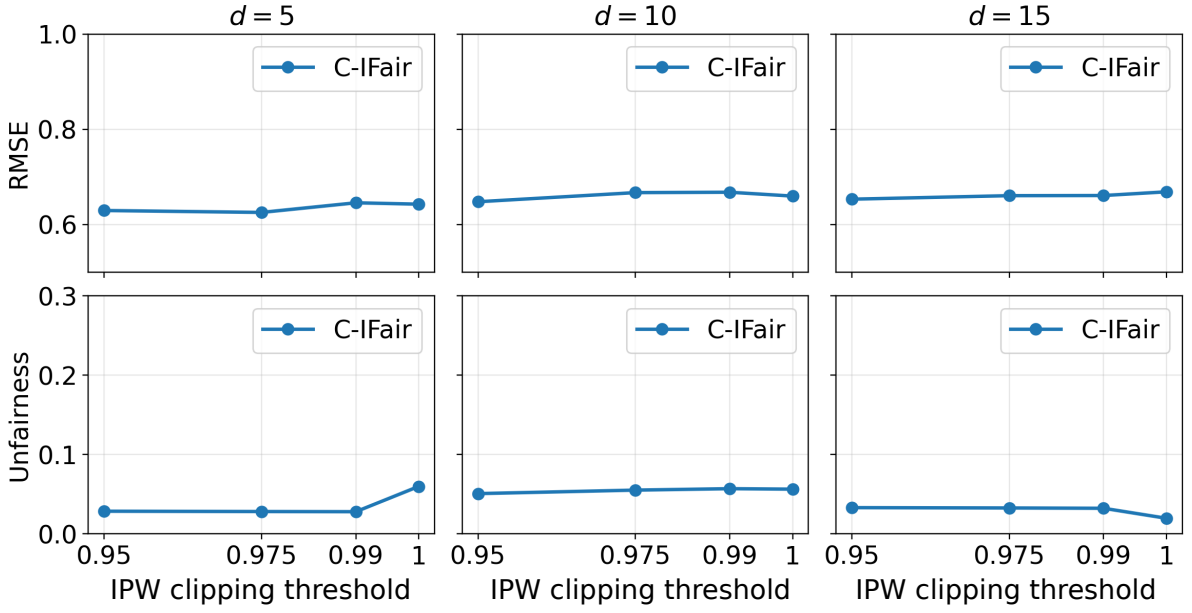


Figure 8: Effect of IPW clipping threshold on performance on linear synthetic datasets with $d = 5, 10, 15$ clusters

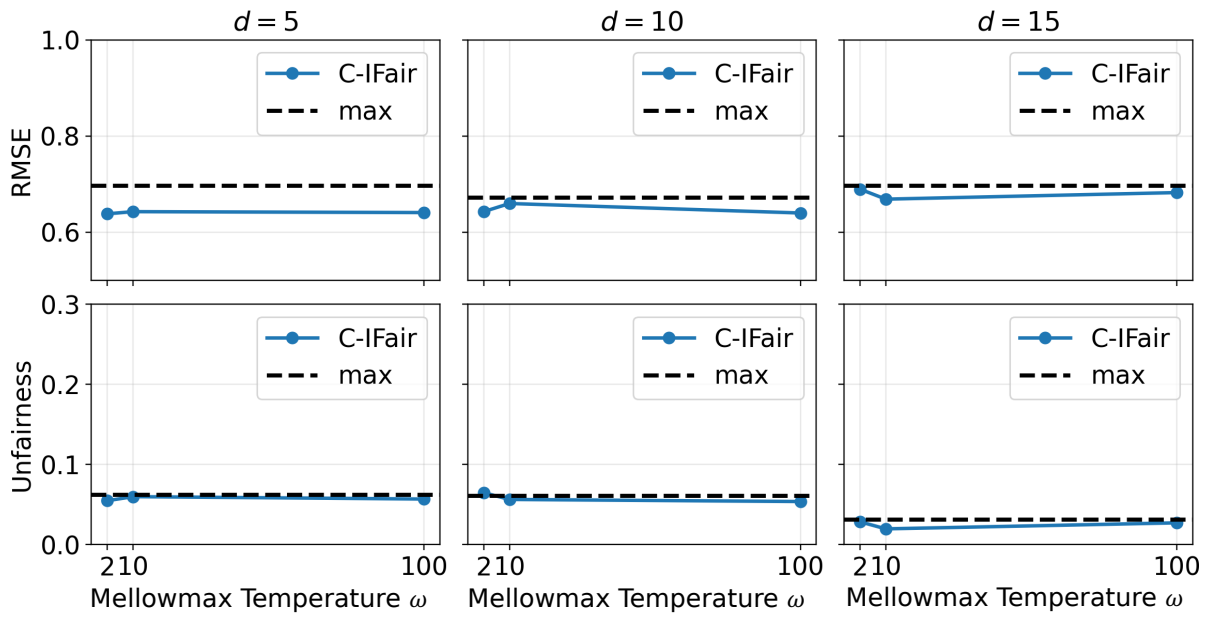


Figure 9: Effect of Mellowmax temperature on linear synthetic datasets with $d = 5, 10, 15$ clusters. Black dashed line denotes variant of our **C-IFair** method that takes maximum over adjustment sets without using Mellowmax.